CHALMERS

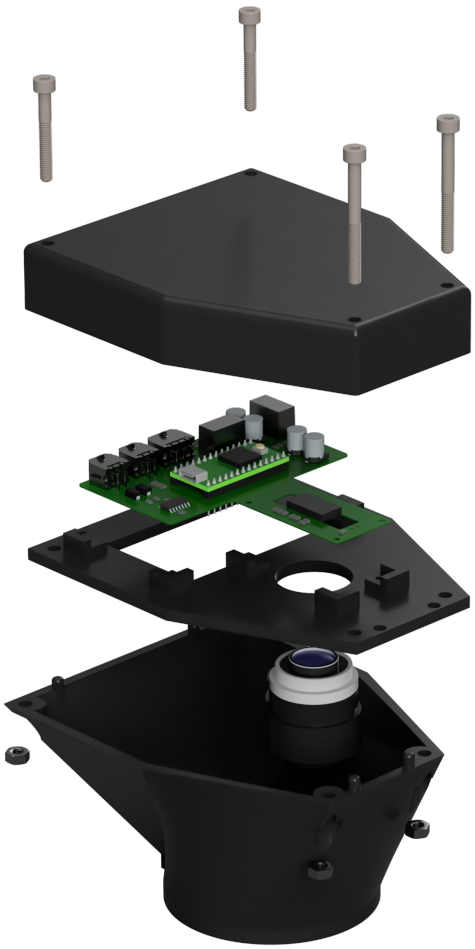

Design and Prototyping of an Optical Non-contact Ground Speed Sensor for a Race Car

A lower cost alternative to commercial Non-contact Ground Speed Sensors for Chalmers Formula Student

Bachelor's thesis in Electrical Engineering

Daniel Eriksen, Linn Henrysson, Lina Levinsson, Casper Lundberg, Milton Runberger, David Spaberg

DEPARTMENT OF Electrical Engineering

CHALMERS UNIVERSITY OF TECHNOLOGY
Gothenburg, Sweden 2025
www.chalmers.se

Bachelor's thesis 2025

Design and Prototyping of an Optical Non-contact Ground Speed Sensor for a Race Car

A lower cost alternative to commercial Non-contact Ground Speed Sensors for Chalmers Formula Student

Daniel Eriksen, Linn Henrysson, Lina Levinsson, Casper Lundberg, Milton Runberger, David Spaberg

CHALMERS

Department of Electrical Engineering
Division of Electric Power Engineering
Chalmers University of Technology
Gothenburg, Sweden 2025

Design and Prototyping of an Optical Non-contact Ground Speed Sensor for a Race Car
A lower cost alternative to commercial Non-contact Ground Speed Sensors for Chalmers Formula Student
DANIEL ERIKSEN, LINN HENRYSSON, LINA LEVINSSON, CASPER LUNDBERG, MILTON RUNBERGER, DAVID SPABERG

Supervisor: Stefan Lundberg, Department of Electrical Engineering
Examiner: Jimmy Ehnberg, Department of Electrical Engineering

Bachelor's Thesis 2025
Department of Electrical Engineering
Division of Electric Power Engineering
Chalmers University of Technology
SE-412 96 Gothenburg
Telephone +46 31 772 1000

Gothenburg, Sweden 2025

Abstract

Precise, non-contact ground speed measurements are crucial in motorsports, where conventional speed measurement methods become inaccurate due to wheel slip. Various contactless methods for measuring ground speed exist, such as Global Positioning System (GPS), estimation using Inertial Measurment Units (IMUs) as well as optical or radar-based sensors. Low latency Non-contact Ground Speed Sensor (NGSS) with sufficiently high enough update rate typically come at a very high cost. This work evaluates several contactless ground speed measurement approaches on how well they could be developed and would fit the requirements of Chalmers Formula Student (CFS). An optical solution based on displacement sensors, commonly used in computer mice, was selected for development. Two displacement sensors with differing specifications were selected and compared under different lighting configurations. The displacement sensor, PAW3395DM-T6QU, was proved to function from 0-120 km/h, outputting speed measurements in both X and Y direction at 100 Hz. The sensor was shown to maintain an error margin below 3.5 % after calibration when tested under controlled environments. This shows the possibilities of using a displacement sensor as a low cost NGSS alternative.

Keywords: Speed, Ground Speed, Speed over Ground, SoG, Sensor, GSS, Non-contact, Optical navigation, Optical flow, Displacement, Motorsport, Formula Student

Sammandrag

Noggranna, beröringsfria markhastighetsmätningar är väldigt viktiga inom motorsport, då de konventionella hastighetsmätmetoderna inte blir tillräckligt exakta på grund av bland annat hjulspinn. Det finns flera beröringsfria metoder för att mäta markhastighet, såsom Global Positioning Systems (GPS), uppskattningar med hjälp av Inertial Measurement Units (IMU:er), samt optiska eller radarbaserade lösningar. Beröringsfria markhastighetssensorer med låg latens och hög uppdateringsfrekvens är dock vanligtvis väldigt dyra. Detta arbete utvärderar flera metoder för beröringsfri markhastighetsmätning utifrån hur väl de kan implementeras samt uppfylla kraven från Chalmers Formula Student (CFS). En optisk lösning baserad på förflyttningssensorer, vanligt förekommande i datormöss, valdes för vidare utveckling. Två sensorer med olika specifikationer valdes ut och jämfördes under olika ljusförhållanden. Förflyttningssensorn PAW3395DM-T6QU visade sig fungera mellan 0-120 km/h och levererade hastighetsmätningar i både X- och Y-led med en uppdateringsfrekvens på 100 Hz. Sensorn visade sig dessutom upprätthålla en felmarginal under 3.5 % efter kalibrering vid testning under kontrollerade förhållanden. Detta visar möjligheten att använda denna typ av sensor som ett kostnadseffektivt alternativ till kommersiella beröringsfria markhastighetssensorer.

Acknowledgements

We would like to take this opportunity to express our gratitude to everyone who contributed to this project.

First and foremost, we extend our thanks to our supervisor, Stefan Lundberg, for his guidance, support, and dedication throughout the entirety of the project. His valuable insights, availability, and commitment were essential to our success.

We are also grateful to Chalmers Formula Student for giving us the opportunity to write this thesis and for their continued support. A special thanks goes to Arthur Alexandersson, William Almqvist and Elias Hedberg for sharing their knowledge and providing insightful input during the course of the project.

Lastly, we would like to thank Douglas Jutsell Nilsson for his assistance in manufacturing the mechanical components required for mounting the wheel on the DC machine, as well as for his help with the actual mounting process.

Daniel Eriksen, Linn Henrysson, Lina Levinsson,
Casper Lundberg, Milton Runberger and David Spaberg

Gothenburg, May 2025

List of Acronyms

Below is the list of acronyms that have been used throughout this thesis listed in alphabetical order:

CAN Controller Area Network

CFS Chalmers Formula Student

CPI Counts Per Inch

FFT Fast Fourier Transform

FPGA Field Programmable Gate Arrays

FPS Frames Per Second

GPS Global Positioning System

LDV Laser Doppler Velocimetry

LED Light Emitting Diode

IC Integrated Circuit

IDE Integrated Development Environment

IR Infrared

IMU Inertial Measurement Unit

IPS Inches Per Second

NGSS Non-contact Ground Speed Sensor

PCB Printed Circuit Board

PLA Polylactide

SoG Speed over Ground

SFV Spatial Filtering Velocimetry

USB Universal Serial Bus

Glossary

Focal length Distance between centre of lens and its focus plane, a shorter focal length yields a greater field of view.

Footprint Outline and pad arrangement on a Printed Circuit Board (PCB) corresponding to a specific electronic component.

Janus configuration A formation where two or more sensors are oriented in opposite or mirrored directions.

LiDAR Method that measures distance by timing a laser's reflection, mapping the surrounding area.

Squat A vehicle body movement, which causes the vehicle's rear to tilt.

Yaw-rate The rotation of a vehicle around its vertical axis.

Contents

1

Introduction

Speed is a common measurement across multiple industries as it is often needed for controlled movement. For regular cars, speed is most often measured using mechanical and electronic speedometers, both of which rely on the rotation of the wheels to measure speed [1]. However, for race cars, this is not ideal since speedometers do not take wheel slip into account. This means that the real speed of the car is not accurate when the wheels slip, which they often do when turning, accelerating or braking heavily during competition [2]. A more accurate measurement of speed is the speed of the ground relative to the car. This is called ground speed, and it can be measured using various methods, such as Global Positioning System (GPS) [3], radar [4], LiDAR [5] and Inertial Measurement Unit (IMU) [6]. They measure a vehicle's speed relative to the ground without the need for physical contact, allowing for accurate speed measurement without the effects of wheel slip [7]. This thesis will refer to them as Non-contact Ground Speed Sensors (NGSSs). For race cars, it is essential to control the slip in order to improve the performance in corners [8]. The cost of a high-end NGSS used in racing typically exceeds 10,000 EUR according to Chalmers Formula Student (CFS). For CFS, spending such an amount is not feasible. The university has provided a budget of 5,000 SEK for this thesis project, which CFS considers a reasonable price.

1.1 Background

Measuring ground speed is especially important for autonomous cars [9]. Since the driving is fully automated, having more accurate information allows the system to make better decisions. In addition, by comparing the contactless ground speed measurement with the rotational velocity of the wheels, the wheel slip can be calculated, which can be used in the control system of the car [10].

This need for precise ground speed data is also relevant in Formula Student, one of the most well-established engineering competitions in Europe [11], where student teams build a formula-style race car and compete in both manual and autonomous driving all over the world. Formula Student provides engineering students with experience in teamwork, project management, and manufacturing. The competition is not only based on having the fastest car, but achieving the best overall performance package, design, and financial and sales planning are also crucial.

CFS is the team representing Chalmers University of Technology in Formula Student. The team is organised into seven groups [12], where each group has their own area of responsibility, covering different aspects of the vehicle. Each year, the team develops and builds a new four-wheel driven electric race car for both manual and autonomous driving to compete in Formula Student all over Europe. In order to improve the overall performance of the CFS vehicle and the autonomous system, an NGSS would be beneficial for the team. The CFS24 car, Freja, which placed 18th in the overall ranking in Formula Student Germany [13], is shown in Figure 1.1.

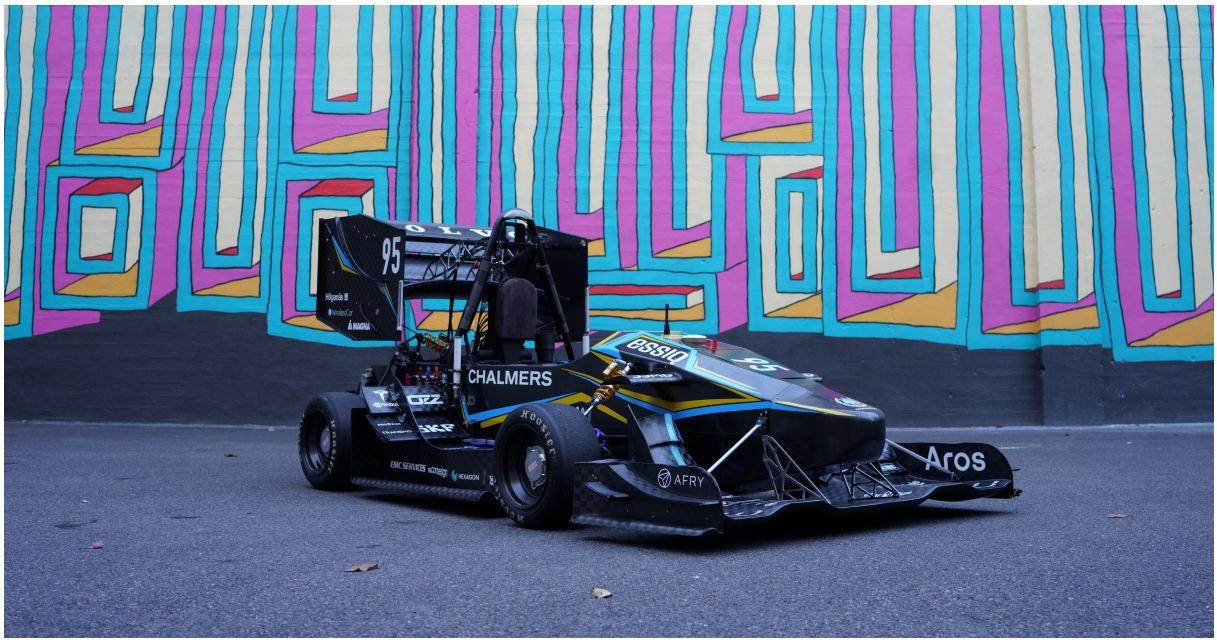

Figure 1.1: Overview of the CFS24 car, Freja. [14]. Adapted with permission.

1.2 List of Requirements from CFS

To meet the needs of the CFS team, the team provided the project with their requirements for the NGSS:

- At least 100 Hz output refresh rate.
- Should tolerate squat and movement of the car body from braking and acceleration.
- Not require calibration after ride height changes (from ≈ 30 mm to ≈ 50 mm).
- Should pass the rain test at the competitions which consists of 120 seconds of water spray [15].
- Should tolerate electrical interference and vibrations.
- Provide raw data using Controller Area Network (CAN) interface.
- Usable when driving over puddles.

- Handle speeds from 0 to $\approx 120\,\mathrm{km/h}$ (0 to $\approx 33\,\mathrm{m/s}$) with an error below $\approx 1\,\%$ to $\approx 2\,\%$.
- Output:
  - Speed in X direction (forward).
  - Speed in Y direction (lateral).
  - Measure rotational velocity of the car around its vertical axis (yaw-rate).

1.3 Purpose

This project aims to evaluate different solutions for non-contact ground speed measurements and to develop a prototype that could eventually be implemented in a future CFS vehicle. Since there are many different ways to solve the same problem, this project will present some of them and their limitations. Using this information, a single solution will be selected for the development of a device designed to measure vehicle ground speed. In addition, the performance of the device will be evaluated.

1.4 Delimitations

A couple of delimitations have been established to ensure the project remains feasible with the allocated resources. Most delimitations were derived from the requirements provided by CFS in Section 1.2. Additional delimitations have been set by the project group to further align the project with the context in which it is developed. The following delimitations have been set:

- Will not consider speeds greater than $\approx 120\,\mathrm{km/h}$ as none of the competitions have tracks with sections that would allow for greater speeds.
- Will only consider mount options less than 300 mm from the ground, as that is where mounting on the car is wished.
- No steps will be taken to ensure water resistance, as the water resistance highly depends on the way the sensor is integrated with the CFS car.
- The output data will not be transformed to counteract the sensor position. This depends on the mounting position and will therefore be left to CFS.
- Will not output yaw-rate. Measuring rotation adds another dimension to the projects, which would take a considerable amount of resources to complete. Besides, yaw-rate is already estimated using IMUs in the CFS car.
- Will only consider solutions mounted directly on the CFS car itself.
- Will not consider LiDAR-based solutions as that is evaluated by another bachelor's thesis.

The sensor's intended use in racing sets some clear delimitations, such as restricting its use to even and flat surfaces like asphalt or concrete. This also means working in a cleaner environment compared to off-road vehicles or cars meant for the road. Therefore, there is no need to worry about how debris and dirt affect the NGSS 's performance to the same extent, simplifying the testing process. However, a limitation when it comes to testing is access to the race car. Since the CFS team is busy with their own development, and taking the race car out for testing requires a significant amount of time and work, this will limit the ability to test the sensor on the race car itself. This will also limit the possibilities of verifying the different requirements in Section 1.2, such as the NGSS's tolerance to electrical interference, passing the rain test, tolerate squat and movement of the car and vibrations created by the car.

2

Methods for Non-Contact Speed Measurement

The following chapter presents different methods for measuring ground speed and explains the underlying theory behind them. This includes a general overview of contactless ground speed measurement, followed by a more in-depth explanation of radar- and optical-based speed measurement as well as Spatial Filtering Velocimetry (SFV) and Laser Doppler Velocimetry (LDV).

2.1 Contactless Ground Speed Measurement

Ground speed, meaning the speed at which the ground is passing under an object, can be measured using several different methods. Each method has its own advantages and disadvantages depending on its application. One of the most common methods is GPS, which is widely used in consumer devices [16]. In motorsports, GPS-based systems are used to track, for example, vehicle performance, laptime and speed [17]. However, these systems often have a lower update frequency and higher latency [18], making them less suitable for real-time speed measurements.

Other sensors with higher update frequencies and greater precision are optical sensors such as those in Kistler's Correvit product series or Sensoric's OMS product series. These sensors are made for vehicle performance testing and offer exceptional performance, but come at a higher cost [19], [20].

Radar-based sensors are a more cost-effective alternative and provide a middle ground between the previously mentioned methods. Radar based ground speed sensors are commonly used in agriculture to provide reliable readings on various surfaces to autonomous farming equipment; most of these are therefore not designed for higher speeds [21].

2.2 Radar Based Ground Speed Measurement

Radar, as explained in [22, p. 4], is an electrical system that consists of a transmitter and an antenna. Radar systems work by transmitting electromagnetic waves towards a surface. The reflected waves are then received by the antenna and processed. By emitting these waves and analysing their reflections, the system can estimate the distance between

the radar and the object. When there is relative motion between the source and the observer, the received signal frequency is shifted (a change in radar frequency). This is also known as the Doppler effect [23]. If the radar device itself is stationary, but an object, such as a car, moves toward or away from it, the radar detects a change in the frequency of the reflected signal. This change, known as the Doppler shift, can be used to calculate the speed and the distance of an object [22]. If, instead the radar is mounted on a moving vehicle and directed toward the ground, the same frequency shift will occur, see Figure 2.1. This allows for a speed calculation and is commonly referred to as Speed over Ground (SoG) radar [24].

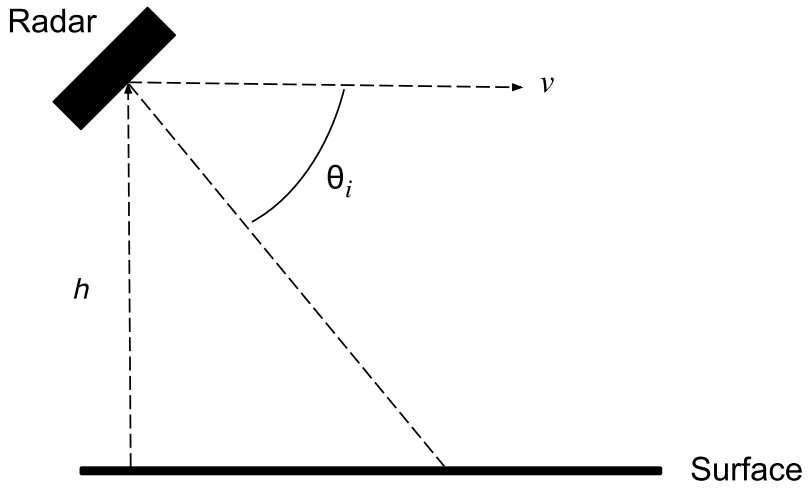

Figure 2.1: SoG radar setup.

Figure 2.1 shows a SoG radar setup with height h and object speed v. The angle of the sensor relative to the ground plane is represented by θ_i, and the Doppler frequency shift is given by

$$f_d = \frac{2v}{\lambda} \cdot \cos\theta_i \tag{2.1}$$

where f_d represents the Doppler shift and λ denotes the wavelength of the transmitted signal [22]. Since f_d depends on the wavelength of the radar, this must be considered when choosing a radar unit to ensure the system performs as expected. Knowing the frequency shift, the speed v can be calculated with (2.1) [22]. However, the obtained speed v only represents movement along the axis of the radar's mounting direction, to obtain a measurement in both X and Y direction, at least two radars would be needed [25].

While most of the past radar modules designated for the automotive industry operate at 24 GHz, modern automotive radars have shifted towards the 77 GHz range. A higher frequency offers several advantages such as more precise speed estimates, longer detection range and reduced antenna size [26].

A project [4], used higher frequency modules to make an NGSS. The hardware used in that project was the TRA120 [27], which is a 120 GHz module. The project used four of these radar modules configured in a Janus configuration to detect the longitudinal and lateral velocity as well as yaw rate. The update frequency of the measurements the sensor gives is 100 Hz. To be able to get the computational speed high enough, a Field Programmable Gate Arrays (FPGA) was used to perform the signal processing and to combine the signals coming from the four different radar modules.

To summarise, radar can be used to construct an NGSS by using the Doppler principle. But to achieve the requirements given by CFS, multiple, high-frequency radar modules would be needed in combination with signal processing that is performed directly in an Integrated Circuit (IC) or on an FPGA.

2.3 Optical Based Ground Speed Measurement

Speed is defined as the displacement of an object over a given time period. Since the displacement can be determined by comparing two consecutive images, a speed can be calculated. Optical methods are therefore common for measuring speed. While image acquisition and resolution may vary, the concept still remains the same.

Different methods for calculating image displacement may include full-field image displacement and template matching, which both are based on cross correlation, where template matching only compares specific regions of the image [28, pp. 81,87]. Figure 2.2 below shows two consecutive frames of asphalt, displayed side by side. The white rectangle represents the specific area that is being matched with the following frame. As can be seen on the right part of the image, the same patch can be found shifted downwards, which corresponds to the displacement. Additionally, there is feature-matching, a method that compares distinct features between frames [29]. High-speed industrial-grade cameras designed with machine vision in mind are typically used in production lines [30]. These capture high-resolution images at high frame rates, allowing for accurate monitoring and automation. These specifications however, also make them suitable for measuring speed [31].

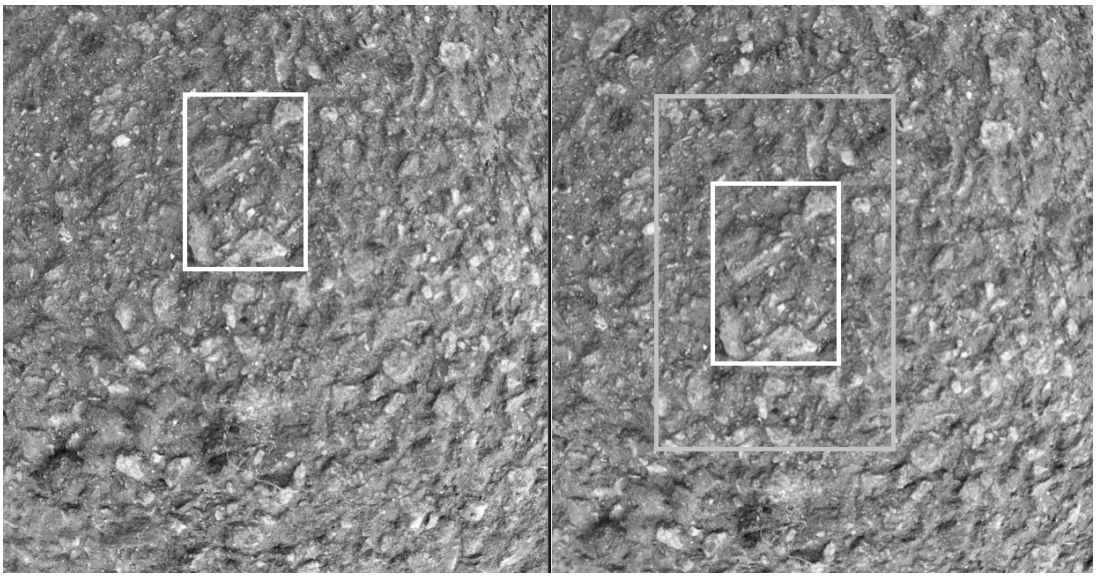

Figure 2.2: Template matching, asphalt (Left: First frame, Right: Second frame).

With a NGSS optimised for performance, a more complex feature-based matching algorithm might not be as suitable [32]. As seen in Figure 2.2, the asphalt has a distinct unique pattern. This works well with a simpler template based matching algorithm that compares the specific regions sequentially. The computational time, therefore, heavily depends on how the camera moved and where the matching started [33]. This could however be optimized even further by making an estimation based on other data to limit the searching area, the larger light gray box represents an example of this. Further optimisation to improve the performance of these algorithms includes implementing neural networks. Although this requires a lot more computational power, the results are shown to be promising [34].

Another method for measuring displacement is by estimation. Multiple models for this exist, and these can be seen as a more general approach with complex theory [35]. As explained in [36], motion can be estimated by assuming that the pixel intensity for the selected pixel and its neighbours remains the same between consecutive frames. Based on these assumptions, equations are derived, which can then be solved to determine a motion vector. More recently, faster machine learning based models have gained popularity, taking advantage of neural networks to instead estimate optical flow [37].

As seen in Figure 2.3, the displacement between frames can be estimated. The red dots with green lines represent individual pixels and their movement trajectories from the previous frame. The larger blue arrow represents the average displacement for all these pixels combined, representing the total estimated displacement for the image sequence.

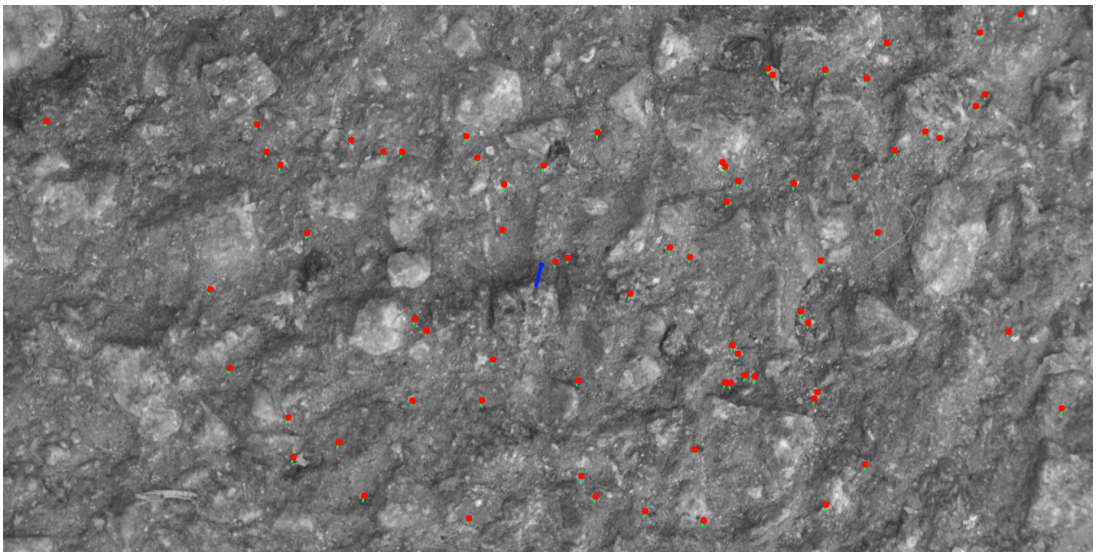

Figure 2.3: Estimated displacement trajectory using OpenCV demo [38].

A simpler approach for finding image displacement is full field cross correlation, a straightforward method that compares pixel intensity across the entire image. The efficiency of these algorithms is typically proportional to the image resolution, as a higher pixel count would increase the amount of comparisons that need to be made [39]. While a higher resolution improves accuracy, it would come at the cost of increased processing time. If the resolution is too low, the algorithm could struggle to find matching patterns. To compensate, even higher frame-rates would be needed. Making most industrial-grade cameras unsuitable as well.

Widely available and inexpensive sensors that calculate change in position based on image displacement are optical navigation sensors or displacement sensors, commonly used in computer mice and drone applications. These have tiny sensors which capture a large number of very low-resolution images and perform displacement calculations directly on the chip [40]. Due to the low resolution, this process is extremely fast and allows for a high update frequency. A comparison in resolution size can be seen in Figure 2.4.

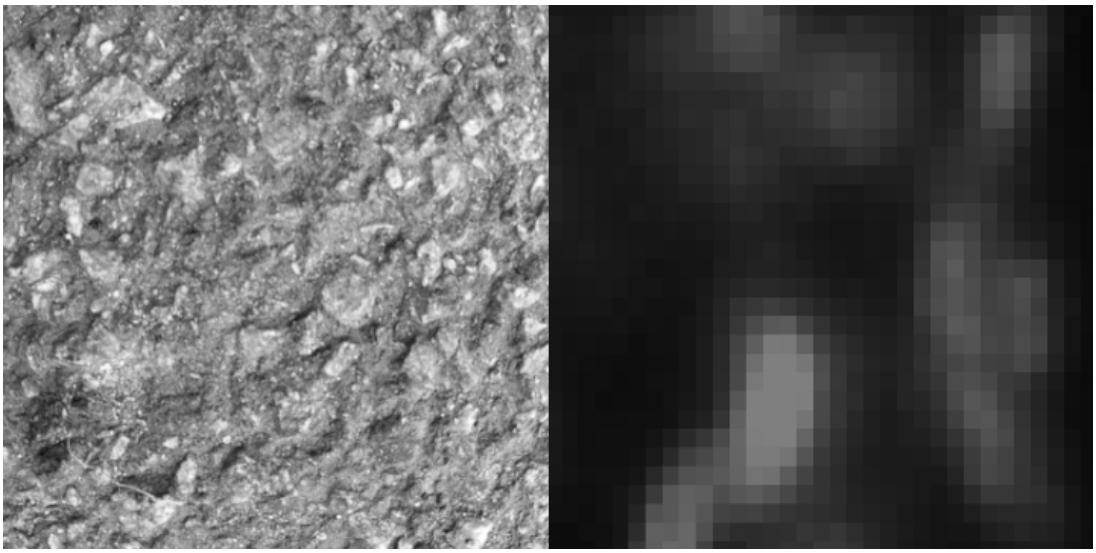

Figure 2.4: Image resolution comparison (Left: Industrial camera: 2048 x 1536 at 50 Frames Per Second (FPS), Right: Optical navigation sensor: 36 x 36 at 7000 FPS).

The sensors used on drones measure flow rate [41], the maximum tracking speed, therefore, depends on the altitude [42]. Which in this application allows for higher tracking speeds. This would therefore be a limiting factor for sensors that are mounted lower to the ground. High-end displacement sensors for intended use in mice however allow for a maximum tracking speed of 650 Inches Per Second (IPS) (16.5 m/s), with minimal distance to the ground [43]. As with drones, increasing the distance between the sensor and the ground surface increases the maximum speed it is capable of measuring. In terms of implementation, these sensors are typically mounted on a Printed Circuit Board (PCB) with an opening beneath the sensor, allowing for direct line of sight onto the tracking surface. A practical implementation of this is presented in [44], where the sensor was mounted at a greater distance from the ground, thereby supporting the possibilities of similar implementations.

2.4 Spatial Filtering Velocimetry

As shown in [45, pp. 5-7], the SFV method functions by illuminating the ground and letting the reflected light pass through a lens. This lens then focuses the reflected light on the spatial filter, which is shown in Figure 2.5.

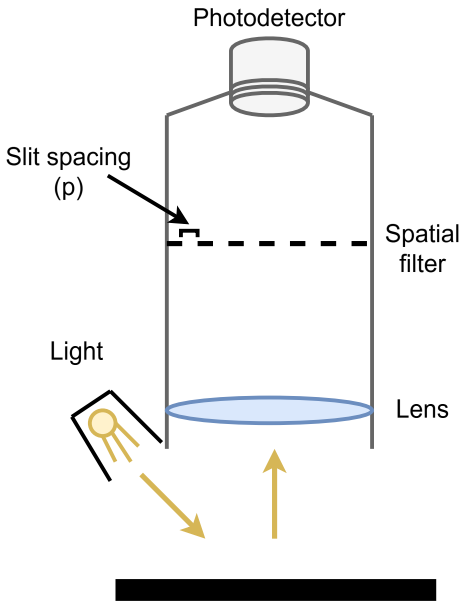

Figure 2.5: The SFV principle.

From Figure 2.5 it can be seen that the spatial filter consists of thin parallel slits with a slit spacing, p. The light passing through the spatial filter is then detected with a photodetector. Due to the movement of the ground and the slit spacing, the intensity of the captured light fluctuates periodically. The output of the photodetector is thus a periodic signal with period T_0 that is proportional to the velocity of the ground, v, through the following formula [45, pp. 5-7]

$$T_0 = \frac{p}{v}.$$

By measuring the frequency

$$f_0 = \frac{1}{T_0}$$

from this signal, the object velocity v_0 is determined from

$$v_0 = \frac{p}{M} f_0,$$

where M denotes the magnification of the lens. Therefore, the velocity is

$$v = M v_0$$

and to obtain the speed, the frequency f_0 must be measured from the output of the photodetector. The signal will contain noise caused by the lens not focusing the reflected light from the ground perfectly on the spatial filter, as well as higher frequency noise from the spatial filter [45, p. 26].

The advantage of the SFV method is that it can be constructed using readily available components. The required components include a spatial filter, a lens to focus the light onto the filter, a photodetector sensor, and a microcontroller or hardware to process the

signal and calculate the frequency from the sinusoidal output of the photodetector [45, pp. 73-74]. However, a key drawback of this method is the signal processing stage, particularly the use of a Fast Fourier Transform (FFT) to determine the signal frequency. FFT calculations can take time, which may lead to a lower update frequency and limit the responsiveness of the system in real-time applications [45, pp. 72-74]. Additionally, input noise, low light intensity, and surface variations can affect the signal processing, all of which can reduce measurement accuracy [46].

In [46], an update frequency of 50 Hz was achieved, demonstrating the feasibility of SFV for real-time measurements. However, improving update rates may require more efficient signal processing techniques or hardware acceleration.

2.5 Laser Doppler Velocimetry

LDV is an optical measurement technique used to determine the velocity of particles within the path of a laser beam with high precision. The method relies on the intersection of two laser beams, which generates an interference pattern within the volume where the two laser beams intersect, as shown in Figure 2.6. As particles pass through this region, they reflect the laser light, creating changes in the interference pattern depending on their velocity [47, p. 11].

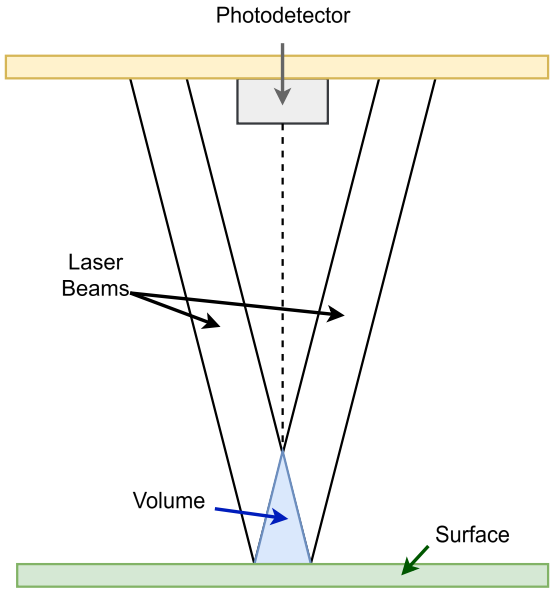

Figure 2.6: The LDV principle.

The same principle applies to surfaces, in which an interference pattern appears, and the velocity of the surface is directly proportional to the modulation frequency of the intensity of the reflected light [48]. The principle of the Doppler effect is applied twice in this process, first, when the incoming laser light interacts with the moving particle, and second, when the reflected light is detected by a photodetector.

By analysing the frequency shift in the reflected light, the velocity of the particle can be accurately determined [47, p. 12]. This technique is used in the field of fluid dynamics and in various industrial applications that require precise velocity measurements [47, p. 1]. The main advantage of using LDV is accurate speed measurement with a high update frequency, with some products managing to achieve an update frequency of up to 1 kHz and are capable of measuring speeds of up to 144 km/h [49]. By using multiple LDVs it is possible to measure both the X and Y directions [50]. Yaw-rate is also possible to measure using the data provided by the LDVs [49].

The main disadvantage of using LDV is that these systems are usually relatively expensive compared to the other methods, with some components costing upwards of 3,000 EUR [51]. Other disadvantages include sensitivity to height variations and interference from dust and water vapour, which would affect the readings of the photodetector [47, p. 287].

3

Method

The following chapter will present the methods for choosing, designing and testing the NGSS. The method was divided into three parts, which consisted of the choice of ground speed measuring method, designing, and finally, testing and validation.

3.1 Choosing Method for Ground Speed Measurement

To decide which ground speed measuring method to implement, a Pugh matrix was used to compare different options based on selected criteria [52]. A literature study was then conducted to gather information about different methods to measure ground speed. The information collected from the literature study was then evaluated following the criteria in the Pugh matrix.

3.1.1 Pugh Matrix Configuration

To support a literature study, a set of relevant criteria for the Pugh matrix was selected based on the requests made by CFS as well as factors that affect the possibilities of completing the project. Each criterion was weighted from 1 to 5 based on importance. The more critical a criterion was, the higher weight it received. Points were assigned to each criterion to evaluate an option and multiplied by the weights to give a total score. All criteria and the reasoning for each weight is shown in Table 3.1 below.

Table 3.1: Explanation for the criteria of the Pugh matrix.

Criteria	Weight	Motivation
Minimal cost	**2**	The project had a budget of 5,000 SEK, but it was not strict, as the institution could provide additional funding if motivated. This criterion, therefore, carried less weight even though the budget was limited.
Minimum procurement overhead	**5**	It was crucial for components to be easily available for purchase through Chalmers. If some were not, they might not have been possible to get at all since all purchases were made through the supervisor of the project.
Minimum steps for physical assembly	**4**	The sensor system needed to be easy to assemble using the resources available at Chalmers. A sensor system that requires special knowledge that the team did not have could be a safety risk, and acquiring the skills could be outside the scope of the project.
Minimum effort for full implementation	**2**	It was less important for the system to be easy to implement, since this project aims to produce a prototype of a concept that could be used, and it would need further development to be implemented in a CFS vehicle.
Minimum design overhead	**3**	It was desirable for the chosen system to need a low design overhead. This was done in order to minimise the occurrence of design errors and for it to take a minimal amount of time. A more complicated design could still have been desirable if the potential of better aligning with the requirements from CFS could be seen.
Meet performance related requirements from CFS	**4**	It was important to meet the performance-related requirements in Section 1.2 (margin of error, update frequency, etc.), so that the data gathered was useful to the car. However, it was not a major issue if the sensor did not meet all the requirements, as its performance could be improved in the future.
Meet the general requirements from CFS	**5**	The sensor was developed for CFS, making it very important to meet the general requirements requested by CFS as some were fundamental design choices that could be difficult to change later (CAN, raw data, tolerate squat etc.). If not met, the NGSS would be incompatible with the car and the needs of CFS.

3.1.2 Literature Study and Evaluation

Based on the criteria set in the Pugh matrix, information was gathered on various methods for measuring ground speed. The information about how these methods work and the evaluations that could be done from the information gathered in the literature study is presented in Chapter 2. The purpose of the literature study was to find methods that could meet the criteria chosen in the Pugh matrix.

With the information gathered from the literature study, several methods potentially suited for the purpose of the project and delimitations were evaluated. Some methods were deemed impractical for specified reasons and were not further evaluated. Methods that could work in practice were further evaluated in relation to all the criteria set for the Pugh matrix. The methods were also compared during the evaluation to establish more reasonable points. All methods were then assigned points for each Pugh matrix criterion. The points in the Pugh matrix were set by the project group with the information in the theory chapter as a guide. The points were then multiplied by their respective weights and summed to give a total score for each solution. The solution with the highest score was chosen for implementation in the project.

3.2 Constructing Prototype

Following the literature study, the designing and prototyping of the NGSS started. This process involved selecting hardware, designing and testing. To support the design decisions, multiple test with different hardware configurations were performed.

3.2.1 Choosing Optics

To keep the functionality of the navigation sensor at increased distances between the sensor and the surface plane, the original optical solution made for short focus distances had to be changed. This was done using a variable focal length C-mount lens from Tamron (13VG2812ASII-SQ). These lenses are typically designed for high-resolution sensors, ensuring that optical quality would not be a limiting factor for the NGSS. The C-mount, screw-thread system also enables easy swapping of lenses and is widely available. Given the sensor's short distance and over-ground speed, a wide-angle lens was necessary.

3.2.2 Choosing Sensor Specification and Light Source

Multiple navigation sensors with different specifications are available. Since these sensors are not intended for this specific application, two models, PAW3395DM-T6QU and PMW3360DM-T2QU (hereafter referred to as PAW3395 and PMW3360), with varying properties, were selected for testing, see Table 3.2.

Table 3.2: Sensor specifications of two selected models, based on manufacturer datasheets, [53], [54].

Name	Tracking Speed (IPS)	Acceleration (g)	FPS	Resolution (CPI)	Step (CPI)
PAW3395	650	50	-	26000	50
PMW3360	250	50	12000	12000	100

As shown in Table 3.2, the main difference between the sensors are their maximum tracking speed, measured in IPS and their resolution and step size measured in Counts Per Inch (CPI). While selecting a sensor with a higher tracking speed may initially seem like the preferred option, it also has some drawbacks. Achieving a higher tracking speed requires a higher frame rate, which in turn limits the sensor's exposure time. Requiring more light to capture images with enough motion data. Both of the sensors have a built in, Infrared (IR) Light Emitting Diodes (LEDs) at 850 nm. This was enough to get a displacement reading from the sensor at the original intended distance, but was found to be too weak when using the modified optics at a greater distance to the ground surface.

Other external lighting solutions, therefore, had to be explored. See the list below:

- Halogen Floodlight (500 W, Broad spectrum)
- IR LED (40 W, 850 nm)
- IR LED (20 W, 850 nm)
- IR LED ($\approx$ 5 W, 850 nm)
- NeoPixel LED Ring ($\approx$ 10 W, Broad spectrum)

Since the sensors were originally designed to operate at 850 nm, some of the solutions may perform better with the sensors than others. To determine what sensor model to choose and what lighting solution would be suitable. A few different tests were made, and these are presented in Section 3.3.

3.2.3 PCB Design

It was decided to design PCBs instead of using breadboards since PCBs are more solid and sturdy. The PCBs were made in *Altium Designer*. To simplify the PCB design, solution diagrams were created to determine which types of components were needed and which connections were required. From the diagrams, it was easier to understand how the schematics should be designed. The PAW3395 and PMW3360 sensors have the same power needs. However, the footprints and pinouts differ. Therefore, the solution model is the same and can be seen below in Figure 3.1.

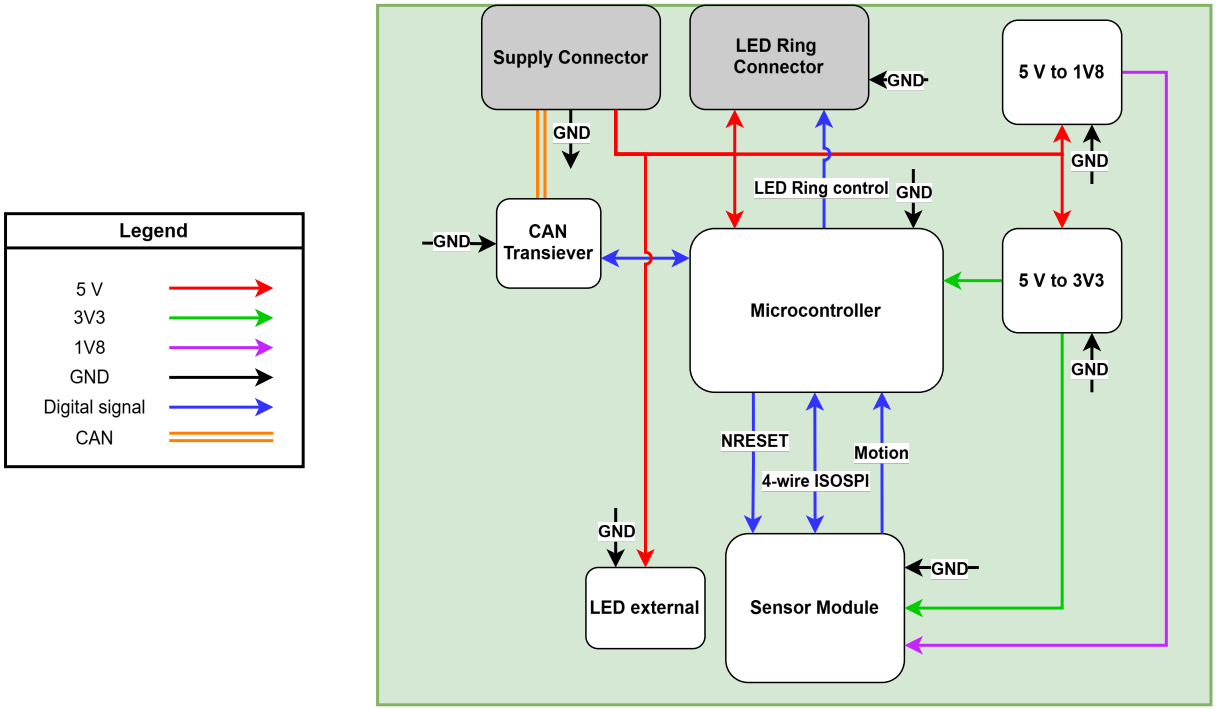

Figure 3.1: Solution diagram for the PCBs with the PAW3395 or the PMW3360 sensor.

From the solution diagram, the schematics and the components for the PAW3395 and PWM3360 sensors were made and chosen, which can be found in Appendix A and B respectively. When the schematics were completed, the layout of the PCB was started. First, the components were placed in an order that allowed the traces to be routed with the shortest distance possible. To protect the ICs, decoupling capacitors were used to prevent electrical energy from transferring from one place to another, and these were placed close to the power pins. The traces for the CAN lines needed to be routed alongside each other. A cut-out was made in the PCB as the image sensor in the displacement sensor needed to see the ground for it to work properly. The PCBs are shown in Figure 3.2 and 3.3.

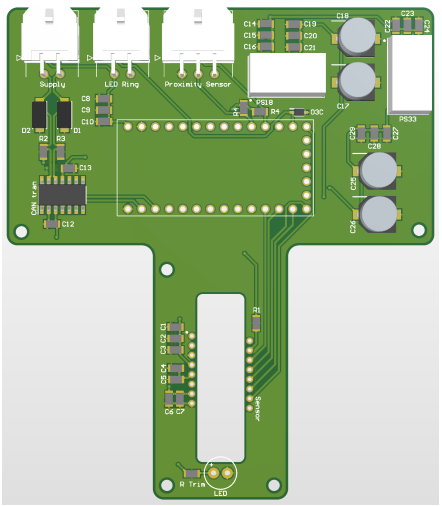

Figure 3.2: The finished design of the PCB for the PAW3395 sensor.

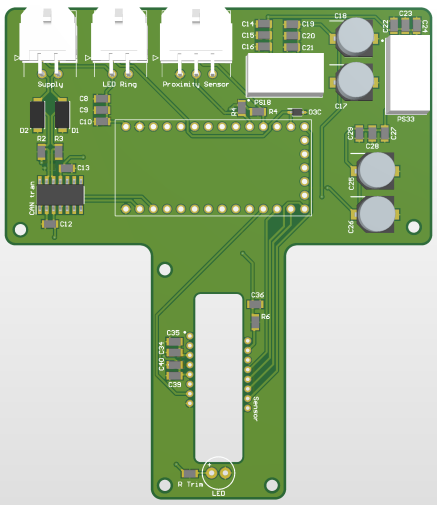

Figure 3.3: The finished design of the PCB for the PMW3360 sensor.

3.2.4 Enclosure Design

The sensor housing was made to enclose and protect the entire system while still maintaining accessibility for both testing and adjustments. The design process involved several steps aimed at ensuring both functionality and protection of the sensor and lens.

1. **Sketching:** Different initial ideas were sketched out and explored. These sketches aimed to explore different ways of protecting the lens while still considering factors such as accessibility, ease of manufacturing, but also assembly and mounting.

2. **Designing:** From the initial sketches, the design for the individual sections took shape and was modelled with CAD software. The dimensions of the housing were determined based on the PCB's dimensions and were designed with 3D printing and assembly in mind.

   (a) **Bottom part:** The bottom part's main function is to protect the lens. It was designed to allow for adjustments to the lens, but also so that a transparent protector can be installed in front of it while letting enough light through. See Figure 3.4.

   (b) **Middle part:** The middle part was designed to have the PCB mounted to it at a slight offset above the surface. To mount the lens, a C-mount thread was incorporated into the design beneath where the displacement sensor optical centre was, which allowed light to pass through and the lens to screw in. See Figure 3.5.

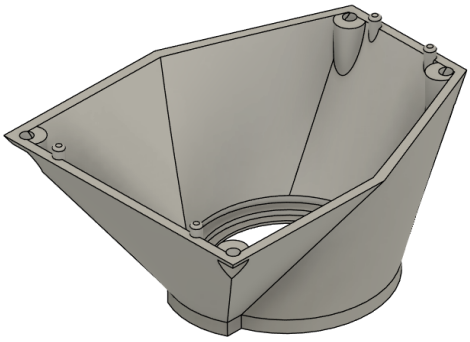

Figure 3.4: Overview of bottom section.

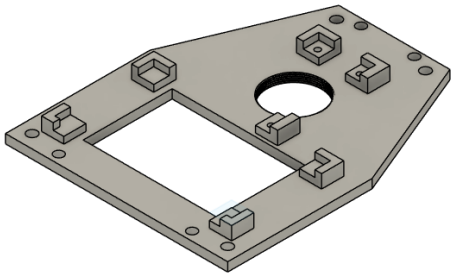

Figure 3.5: Overview of middle section.

   (c) **Top part:** A top part was designed as a lid in two different versions, one for the final enclosure and one with the test rigs in mind.

      i. **Standard version:** The main version was instead designed to enclose the entirety of the system, and protect the electronics. However, it also had to have a connection port for CAN communication and power. See Figure 3.6.

ii. **Test Rig:** This version was designed to be mounted on the test rigs. It was therefore designed in such a way that it could easily be mounted and would allow for access to the PCB, cable connections and lens during testing. See Figure 3.7.

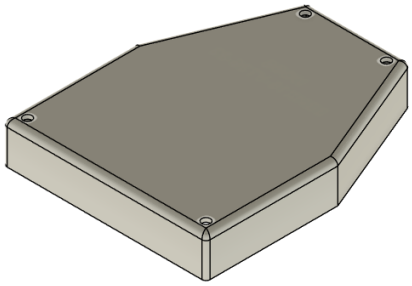

Figure 3.6: Overview of top section.

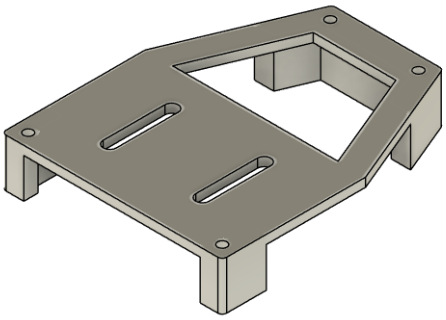

Figure 3.7: Overview of top section for test rig.

3. **Manufacturing:** The parts were 3D printed using Polylactide (PLA). A circular lens filter was glued to the bottom of the housing, protecting the lens and letting light through.

4. **Assembly:** Once all the sub parts were designed, they were pressed together using screws alongside the outer edge. This method was chosen to allow for easy disassembly and the possibility of re-designing individual sections during testing.

3.2.5 Software Design

The software for the project was designed to run on the Teensy microcontroller on the PCB. *PlatformIO*, which is an Integrated Development Environment (IDE) for programming microcontrollers, was used to build and upload code to the Teensy. The code was written in C++ to be compatible with *PlatformIO*. The code was structured into three parts, where one part controls the communication with the displacement sensor, another handles the CAN communication and the main part that combines these parts to output the sensor readings.

The sensor driver is the part that handles the communication with the displacement sensor. Two different sensor drivers were written to communicate with the PAW3395 and PMW3360 displacement sensors. The drivers were constructed by following the respective data sheet [53], [54]. The following functions in Table 3.3 were implemented in both drivers to be able to acquire the relevant data from the displacement sensor needed to calculate the speed, configure and test it. These functions have the same functionality but have different implementations depending on the displacement sensor. The only function that differs between the displacement sensor drivers is the lift cut-off function. For the PAW3395, the lift cut-off is set to 2 mm since that is the highest value it can be, and for the PMW3360, the highest value it can be is 3 mm.

Table 3.3: Functions for acquiring data from the displacement sensors.

Function	Functionality
set_register	This function enables our program to write values into a specified register on the displacement sensor.
read_register	This function makes it possible to read values from different registers on the displacement sensor.
get_speed	This function calculates the speed from the displacement data from the displacement sensor.
print_displacement	print_displacement sends the displacement values given from the displacement sensor on the Universal Serial Bus (USB) port. This function is used for testing.
raw_data	The function rawData collects an image from the image sensor and returns it as an array.
print_raw_data	print_raw_data sends the rawData values on the USB port and is used for testing.
lift_cutoff_2mm	This function sets the lift cutoff to 2 mm and is only implemented on the PAW3395 displacement sensor.
lift_cutoff_3mm	This function sets the lift cutoff to 3 mm and is only implemented on the PMW3360 displacement sensor.
init_chip	This is an initialisation function to get the displacement sensor started.

The second part handles all communication using the CAN bus. A number of functions for sending messages and a system for handling incoming messages were implemented. Initially, the sensor does not send anything on the CAN bus, and it only listens for incoming messages. When receiving a message, the sensor checks if the ID of the sender match any of the ones it should listen to. For testing purposes, the only valid ID is 23. In reality, these IDs would be set by CFS when adding the sensor to the car. When a valid message is received, it is handled according to the first byte of the message's buffer. See Table 3.4 for all handled requests. The CAN interface was built for continuously sending messages on the CAN bus. The sensor, therefore, checks how long it has been since the last sent message every iteration and sends the correct messages when time is due.

Table 3.4: CAN communication functionality.

Request value	**Triggered functionality**
110	The sensor runs **set_speed_write(true, message_buffer)** which makes the sensor start sending the speed on the CAN bus with the interval specified in the second value in the buffer.
100	The sensor runs **set_speed_write(false)** which makes the sensor stop sending the speed on the CAN bus.

The main part of the program consists of a program loop and a setup function. The setup function runs once when the program is started, and the loop function runs continuously. In the setup function, initialisations for the CAN communication and displacement sensor are run. In the loop function, the program is listening for CAN messages that come from the rest of the car and handles them. If the NGSS is set to measure the speed, it will continue sending the speed on the CAN bus until it gets an instruction to stop. The messages communicating the speed are by default sent with a frequency of 100 Hz. The output frequency could be set higher, but limitations of the displacement sensor might occur. In Figure 3.8, a flowchart describing the program process when measuring speed can be seen. For testing purposes, USB communication with the microcontroller was used to read data from the test functions in the displacement sensor driver.

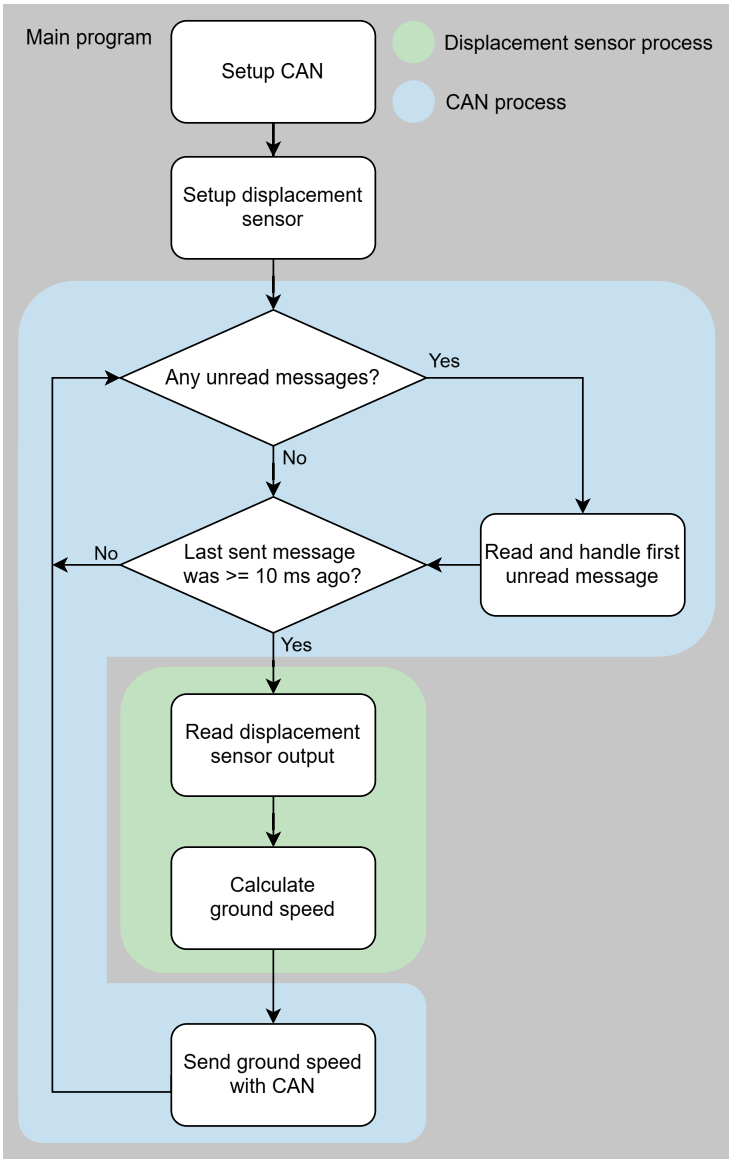

Figure 3.8: Flowchart of the main program loop when the sensor is configured to measure speed.

3.2.6 Construction of Test Rig

To ensure more consistent testing, three custom test rigs were constructed. The first rig was built using a shelf trolley, see Figure 3.9. The NGSS was then mounted to the rig, alongside the lighting solution, all of which could be adjusted in height and position as needed. This setup enabled adaptable and repeatable testing across different surfaces in both X and Y direction.

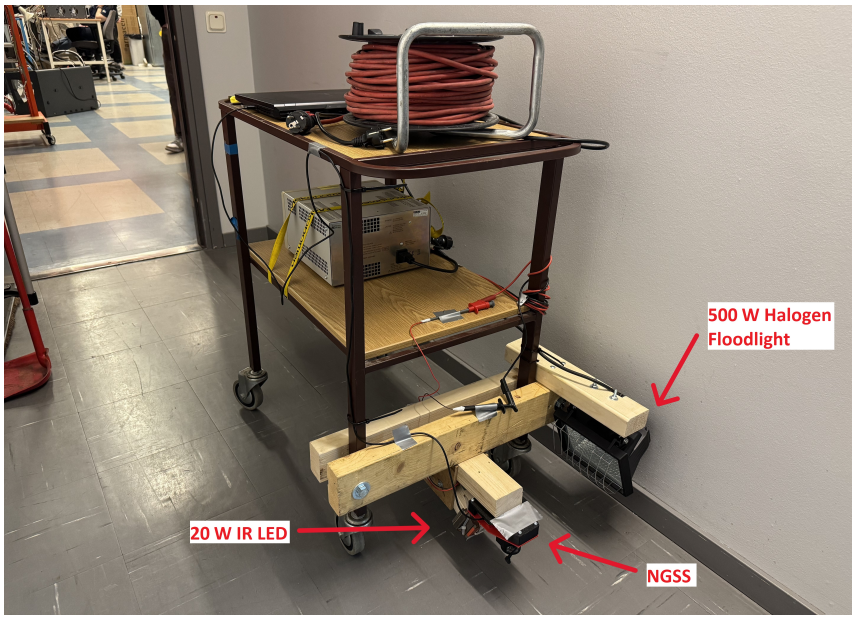

Figure 3.9: Overview of the shelf trolley test rig.

The second rig was constructed for tests that required a constant speed. A car wheel was mounted onto a large electric motor with adjustable speed control, see Figure 3.10. The sensor and external lighting solutions were fixed to the test bench, with an adjustable distance to the wheel. To better simulate an asphalt-like surface structure, the wheel was coated with coarse sandpaper.

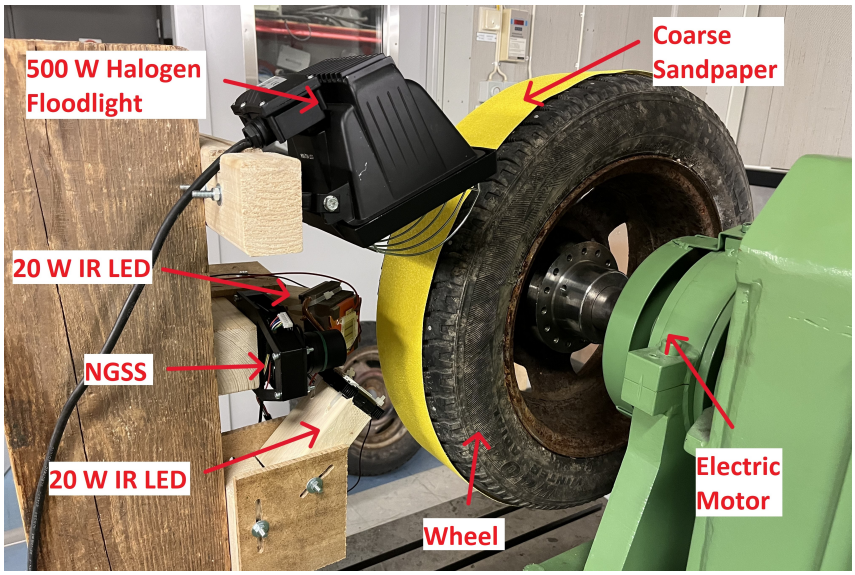

Figure 3.10: Overview of the electric motor test rig.

The final rig was constructed to mount the sensor to a car, and in this way, higher speeds on asphalt could be tested. The frame was constructed from two plywood sheets with holes in them. The sensor and lighting solution could then be screwed into this frame and

with bolts be squeezed around the tow-bar, resulting in the sensor hanging slightly above the ground as intended. See Figure 3.11.

Figure 3.11: Overview of the car mount.

3.2.7 Calculating Speed from Displacement

To calculate the speed from the displacement output of the displacement sensor, the following formula was used

$$speed = height\_speed\_scaling \cdot \frac{displacement\_mm}{delta\_time}$$

where

$$height\_speed\_scaling = height\_factor \cdot height$$
$$displacement\_mm = displacement\_CPI \cdot CPI\_to\_mm\_factor.$$

The $displacement\_CPI$ value is the displacement value continuously retrieved from the displacement sensor at a resolution of 5,000 CPI. A conversion factor was used to calculate the displacement into millimetres. This factor was calculated by dividing how many millimetres there are in an inch and dividing that by the CPI value. This gave the value

$$CPI\_to\_mm\_factor = \frac{25.4}{5000} = 0.00508.$$

To get the $height\_speed\_scaling$, the mounting height (in millimetres) of the sensor was multiplied by a factor ($height\_factor$). This factor was initially set to 1 before calibration. Calibration was done by comparing the sensor output speed with the known constant speed for a set of speeds across the entire speed range and averaging the offset for all measurements. The $height\_factor$ could then be replaced, and would make the sensor output match the actual speed. The $height\_speed\_scaling$ was multiplied by the displacement and divided by the time since last measurement ($delta\_time$) in milliseconds, resulting in a speed output in m/s.

3.3 Testing

The following sections describe the tests conducted to support key design decisions, including the selection of a displacement sensor and light source, as well as assessing performance. Each of the test configurations is explained and summarised in tables.

3.3.1 Assessing Sensor Linearity Across Speed Range

To assess the performance of the sensor across the entire speed range, measurements were performed with the test rig shown in Figure 3.10. The rotational speed of the wheel ranged from 50 RPM to 1150 RPM, in increments of 50 RPM. Both modules were tested using a 40 W IR LED as the light source. For each measurement, the speed was held constant, and 1000 measurements were averaged. 50 RPM roughly corresponds to 1.5 m/s and 1150 RPM which roughly correspond to a surface speed of 35 m/s, which covers the speed range of the CFS car. An overview of the tested configurations is shown in Table 3.5.

Table 3.5: Configurations for speed range and relationship tests.

Sensor Model	Light Source	Speed Range (RPM)	Step (RPM)
PAW3395	40 W IR LED	50 – 1150	50
PMW3360	40 W IR LED	50 – 1150	50

To visualise the results, the speed measurements for each speed were plotted against the rotation speed. A trendline was applied to assess the relationship between the sensor output and known speed. Deviations from this line could indicate non-linear behaviour, measurement inaccuracy or measurement errors. The actual surface speed was also compared to the sensor output. The scaling, *height_factor*, was calculated for each of the displacement sensors for the given height.

3.3.2 Evaluation of Light Sources

To determine a suitable external light source for reliable sensor readings across the entire speed range, both displacement sensor models were tested under five different lighting conditions. The tests were performed at two constant speeds, 100 RPM and 1000 RPM, which corresponds roughly to 3 m/s and 30 m/s respectively for a duration of 10 seconds. These speeds were selected to represent both low and high-speed scenarios. A summary of the configurations is shown in Table 3.6

Table 3.6: Configurations for light source testing.

Sensor Model	Light Source	Speeds (RPM)
PAW3395	500 W Halogen Floodlight	100, 1000
	40 W IR LED	100, 1000
	20 W IR LED	100, 1000
	5 W IR LED	100, 1000
	NeoPixel LED Ring	100, 1000
PMW3360	500 W Halogen Floodlight	100, 1000
	40 W IR LED	100, 1000
	20 W IR LED	100, 1000
	5 W IR LED	100, 1000
	NeoPixel LED Ring	100, 1000

The sensor outputs for each of these combinations were visualised using box plots. The deviation from the expected reading could then be compared between the sensor modules and different light sources to evaluate the effects that illumination has on accuracy and noise.

3.3.3 Height and Focus Evaluation

During use, changes in height could occur. For example, changes in ride height and suspension travel. To assess how this might affect the sensor output, measurements for a set constant speed of 500 RPM, which corresponds to 15 m/s, were done with the PAW3395 for multiple distances from the surface. A 40 W IR LED was used as a light source, and for each point, 1000 measurements were averaged. The setup is summarised in Table 3.7 below.

Table 3.7: Test configurations for height dependency evaluation.

Sensor Model	Light Source	Speed (RPM)	Distance (mm)	Step (mm)
PAW3395	40 W IR LED	500	30 – 135	5

After plotting, a polynomial was fitted to the data points. This shows the relationship between the distance over ground and speed output by the sensor, allowing for scaling changes to be made to the outputted measurement to display a correct speed if the height is known.

3.3.4 Impact of Pinhole Cover on Sensor Output

Both sensor models have a pinhole acting as a lens, limiting light intake. This is built into the underside cover of the IC and can be removed with a pair of pliers, exposing the entire image sensor. See Figure 3.12 below.

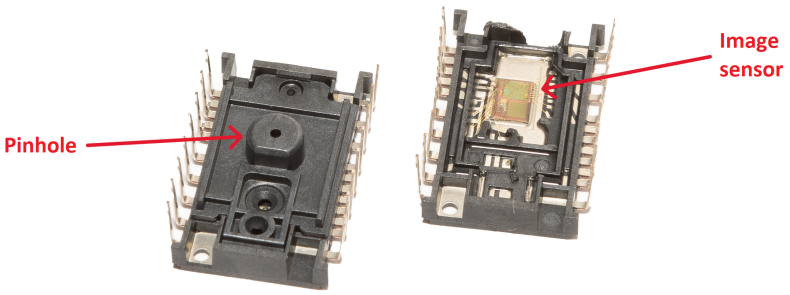

Figure 3.12: Underside view of PAW3395 with and without pinhole cover.

This allowed image focus to be calibrated for even shorter distances to the ground than with the pinhole in place. To compare if these configurations affected anything other than focus, measurements were performed at two constant speeds (100 RPM and 1000 RPM) for a duration of 10 seconds under two different lighting conditions. See Table 3.8. The recorded data was then compared with box plots to evaluate any deviation between the configurations.

Table 3.8: The configuration for testing with and without the pinhole.

Sensor Model	Light Source	Speeds (RPM)
PAW3395 (Original)	40 W IR LED	100, 1000
	20 W IR LED	100, 1000
PAW3395 (No pinhole)	40 W IR LED	100, 1000
	20 W IR LED	100, 1000

3.3.5 Testing on Asphalt

Tests were also conducted on asphalt to ensure that the sensor would perform as expected on the surface it was intended for. Initial tests were carried out using the trolley test rig. Since it was not possible to maintain consistent or known speeds with this setup, the primary objective was to verify that the surface and lighting solution would provide continuous displacement readings.

Testing on asphalt at higher speeds and under conditions closer to those on the race car required it to be mounted to a car. A driving sequence that included acceleration up to $\approx 33\,\mathrm{m/s}$, consistent speed using cruise control and a shorter deceleration was used. The configurations for both of these tests can be seen in Table 3.9 below.

Table 3.9: Asphalt test configuration on the car.

Sensor Model	Light Source	Setup
PAW3395 (No pinhole)	20 W IR LED	Trolley
PAW3395 (No pinhole)	Sunlight	Car

4

Results

The following section will present the results that were made throughout the different stages of the project. The result contains the choice of speed measuring method, the tests that were conducted for the different components in the NGSS and the tests for evaluating the performance of the NGSS. The final hardware design is also presented at the end of the section.

4.1 Selecting Ground Speed Measurement Method Using Pugh matrix

The different ground speed measuring methods that seemed to meet the criteria well was included in the Pugh matrix, shown in Table 4.1. This meant that LDV was not included since it was deemed too expensive to implement. These methods were then scored on how well they met each of the selected criteria. Since the criteria in the Pugh matrix are broad, the point each method got on each criterion was set by the project group, with the knowledge that had been acquired during the literature study as a basis. This meant that each point was set in a subjective manner.

Table 4.1: Pugh matrix showing the evaluation for different ground speed measuring methods.

Criteria	Weight	Radar - Doppler	Optical - Standard camera	Optical - Spatial filtering	Optical - Navigation sensor
Minimal cost	2	2	1	5	3
Minimal procurement overhead	5	2	3	3	4
Minimum steps for physical assembly	4	4	3	2	3
Minimum effort for full implementation	2	4	2	3	3
Minimum design overhead	3	1	2	3	4
Meet the performance related requirements from CFS	4	5	4	4	4
Meet the general requirements from CFS	5	5	4	4	4
	Sum	**86**	**75**	**84**	**92**

As seen in Table 4.1, the optical navigation sensor achieved the highest score. Therefore, it was the sensor type that best fit the weighted criteria. Based on the result from the Pugh matrix, the optical navigation sensor was then chosen as the solution to be developed for the NGSS.

4.2 Test Results

The following sections present the results of the various tests that were done on the NGSS. The results primarily focus on the differences between the PMW3360 and the PAW3395 displacement sensors and how they performed under different lighting conditions.

4.2.1 Assessing Sensor Linearity Across Speed Range

Figure 4.1 shows the speed range measured by the two sensors, PAW3395 and PMW3360 across a range of different RPM values. The measurements were taken at a mounting height of 80 mm with a 40 W IR LED as a light source.

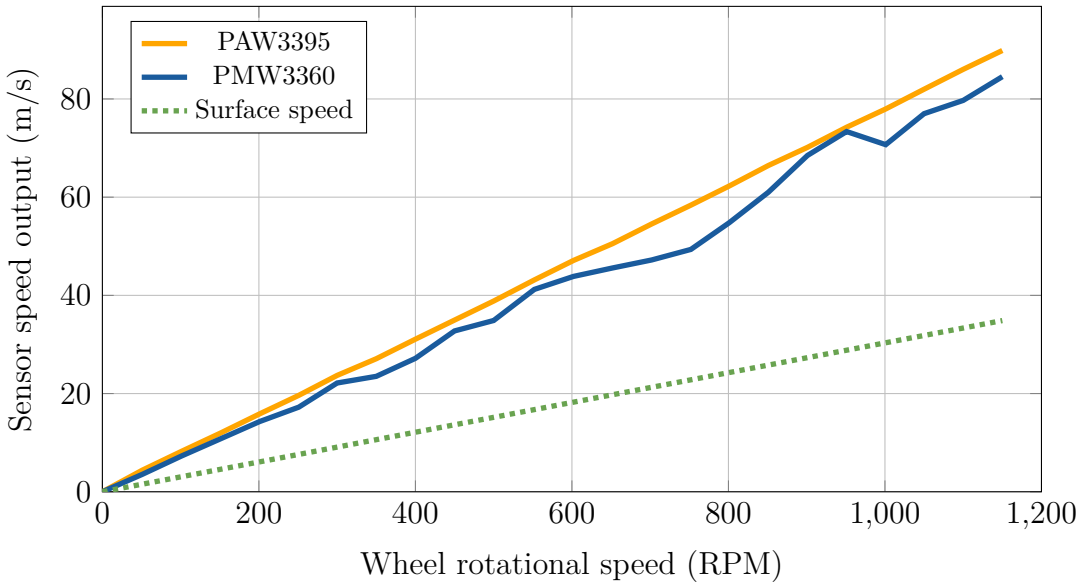

Figure 4.1: Speed ramp-up at height 80 mm.

The speed output for the two displacement sensors, after calibration, is shown in Figure 4.2. Using a *height_factor* of 0.3861 and 0.4264 for PAW3395 and PMW3360 respectively, at a mounting height of 80 mm.

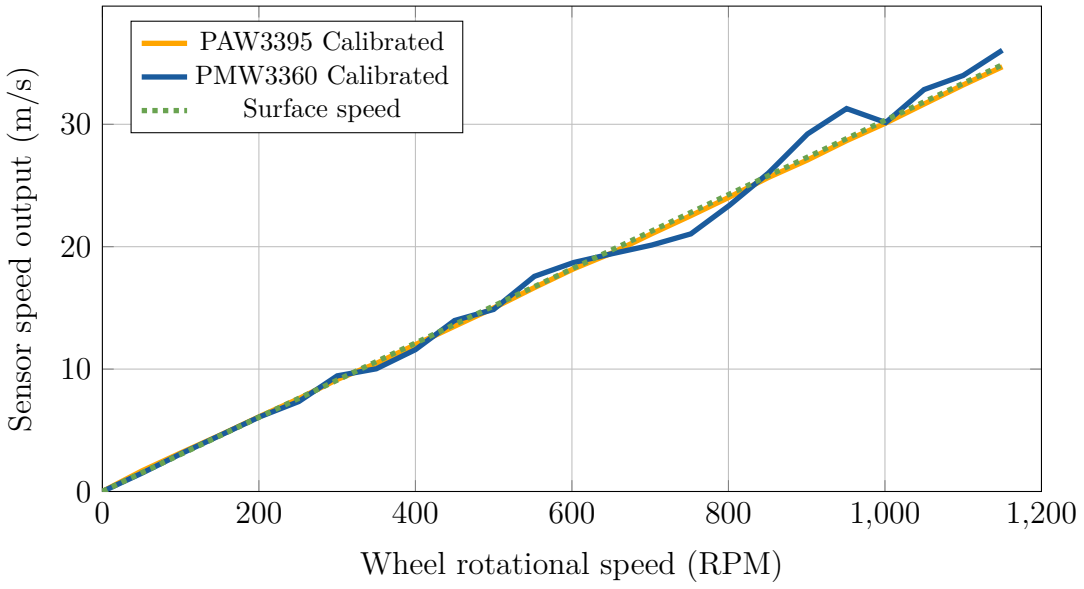

Figure 4.2: Calibrated speed ramp-up at height 80 mm.

For validation, an additional ramp-up test was performed on the PAW3395 sensor using the same configuration as before. If the behaviour is consistent, the sensor output should correspond to the surface speed as in Figure 4.2. The result is shown in Figure 4.3. After applying scaling with the *height_factor*, the output speed aligns with the reference surface speed as expected. The highest observed deviation is 1.04 m/s, appearing at higher RPM values.

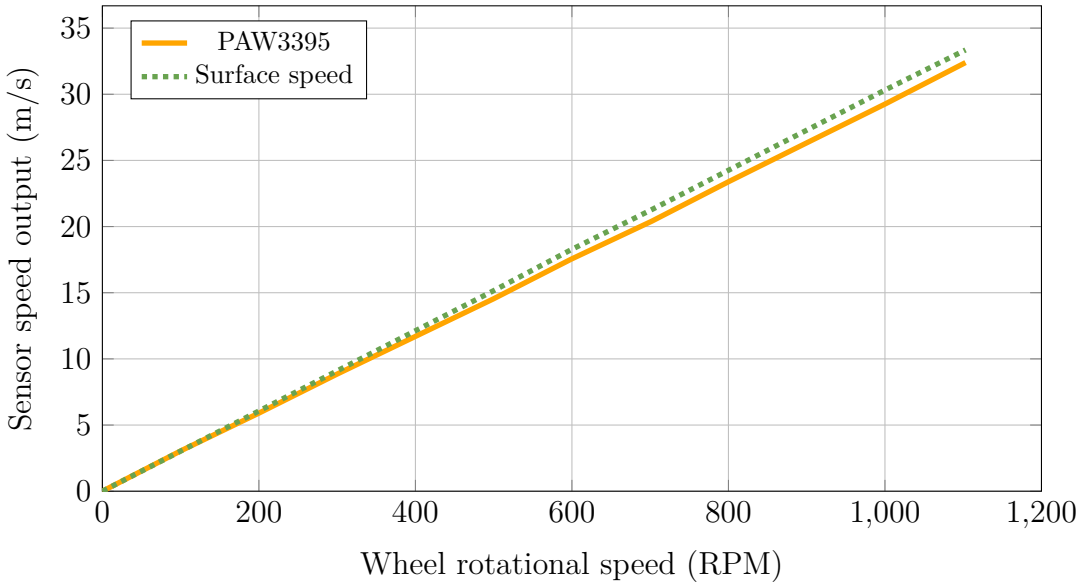

Figure 4.3: Speed ramp-up validation at height 80 mm.

4.2.2 Evaluation of Light Sources

Out of the other external lighting solutions that were tested, both the IR LEDs at 5 W and the NeoPixel LED Ring were not bright enough to get any displacement readings. The surface illumination of the three other lighting methods were however strong enough to get speed measurements. Figure 4.4 shows box plots visualising the distribution of measured speeds under different lighting conditions by both the PAW3395 and PMW3360 during a period of 10 s. Each box represents the interquartile range (25th to 75th percentiles), with whiskers extending to values within 1.5 times the interquartile range. Data points outside this range are considered outliers and are visualised as individual dots. The sensor was mounted 80 mm above the testing wheel, which in this case had a speed of 100 RPM, corresponding to a surface speed of approximately 3 m/s. The *height_factor* was set to 0.3861 for PAW3395 and 0.4264 for PMW3360.

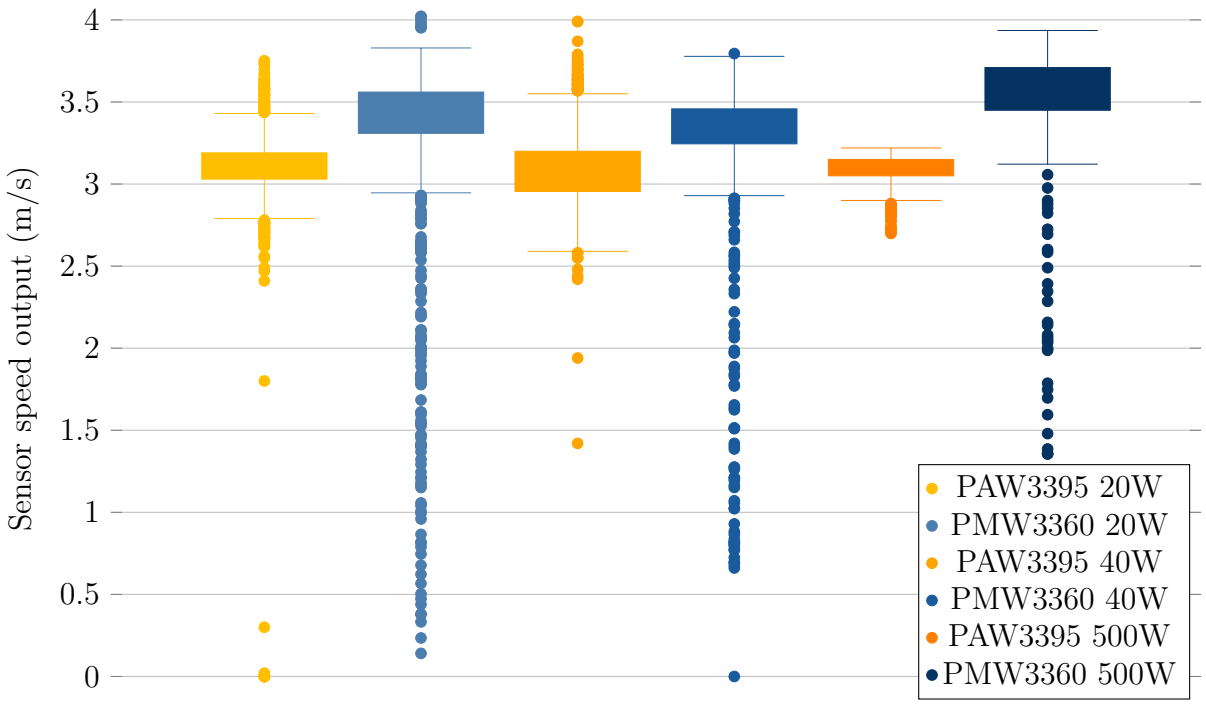

Figure 4.4: Sensor deviation for PAW3395 & PMW3360 for different light sources at 100 RPM.

The same lighting solution tests were also done at 1000 RPM, corresponding to a surface speed of approximately 30 m/s with the same parameters as the tests at 100 RPM. This can be seen in Figure 4.5.

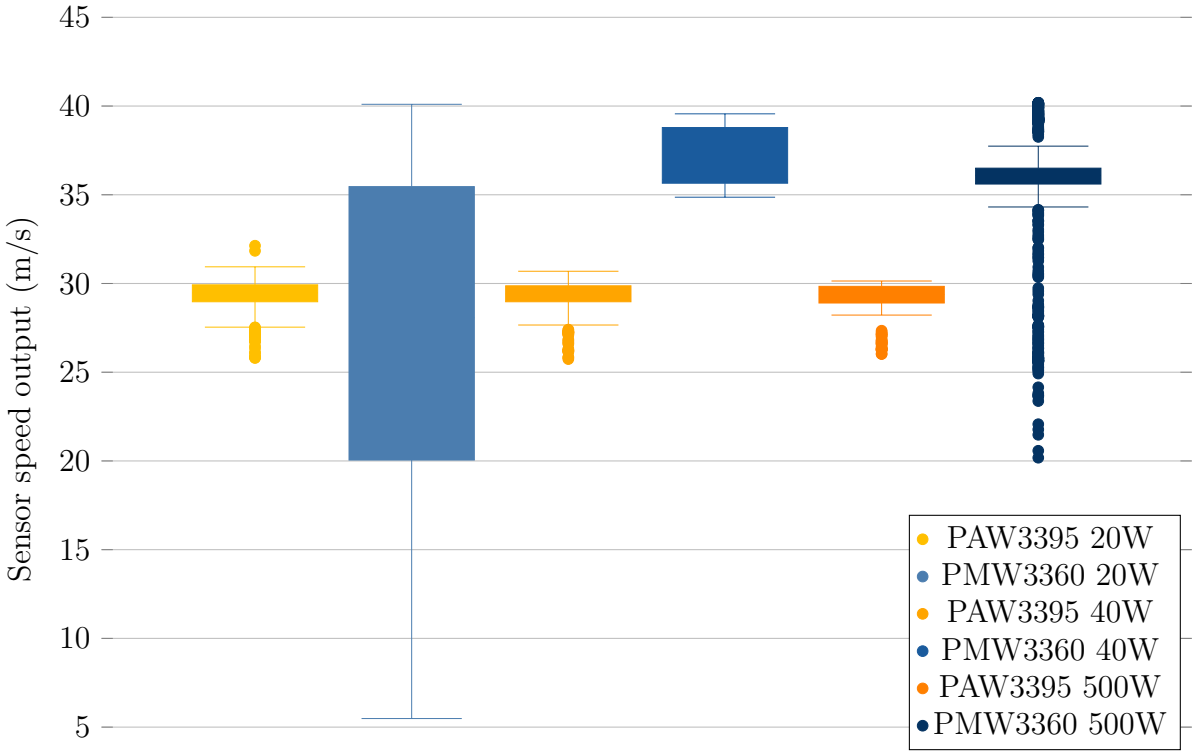

Figure 4.5: Sensor deviation for PAW3395 & PMW3360 for different light sources at 1000 RPM.

4.2.3 Height and Focus Evaluation

Figure 4.6 shows the measured sensor output as a function of distance to the ground surface. Measurements taken at distances less than 40 mm and greater than 125 mm resulted in either noise or were unable to output any readings. Measurements between 40 mm and 60 mm varied, but became more consistent for greater distances up to 125 mm.

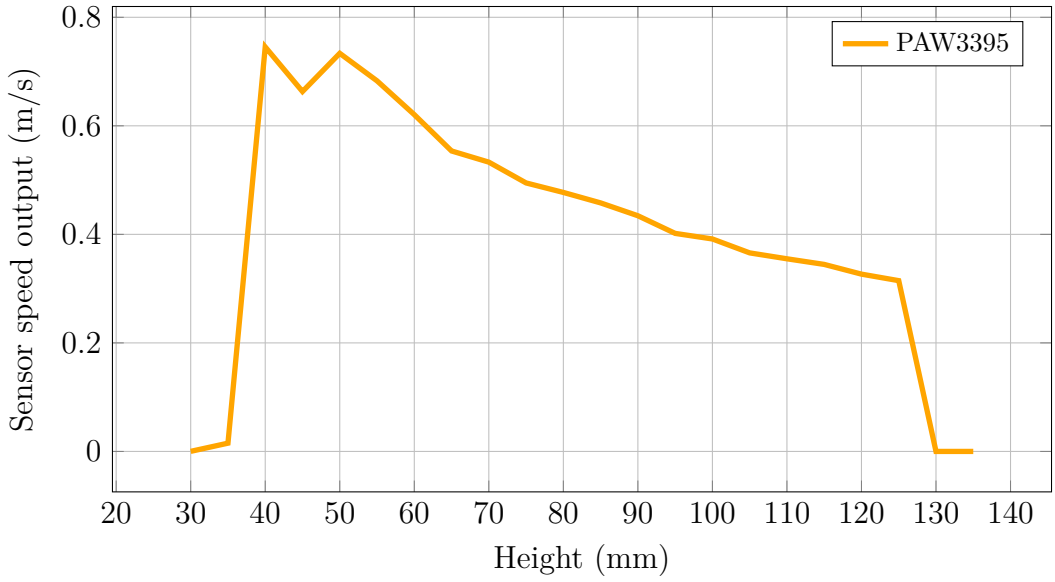

Figure 4.6: Speed output as a function of height at different heights without any calibration.

For the range 50 mm to 125 mm, a polynomial curve was fitted to the ratio between the measured speed and the true speed (*ratio = true_speed / measured_speed*), as shown in Figure 4.7. The equation for the curve is $ratio = -0.00015548 \cdot height^2 + 0.38937290 \cdot height + 1.74291411$. The curve was used to verify that the sensor would output a consistent reading, regardless of height, for the range 50 mm to 125 mm. See Figure 4.8.

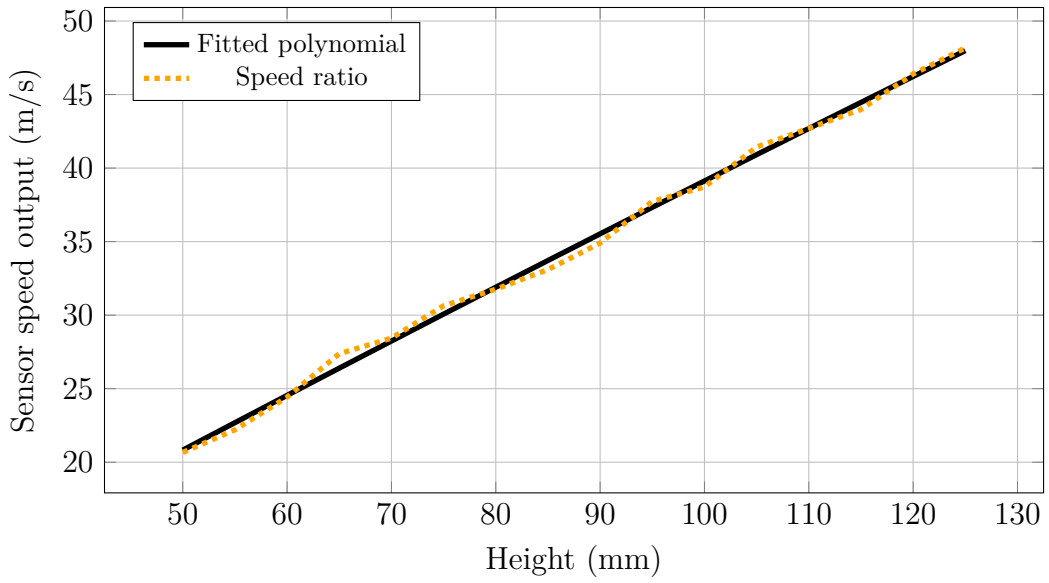

Figure 4.7: Polynomial curve fitted to the ratio between measured speed and true speed for different heights.

In Figure 4.8 below, the comparison between the calibrated speed with the true speed shows the biggest error ≈ 3.4 % and the average error ≈ 1.2 %.

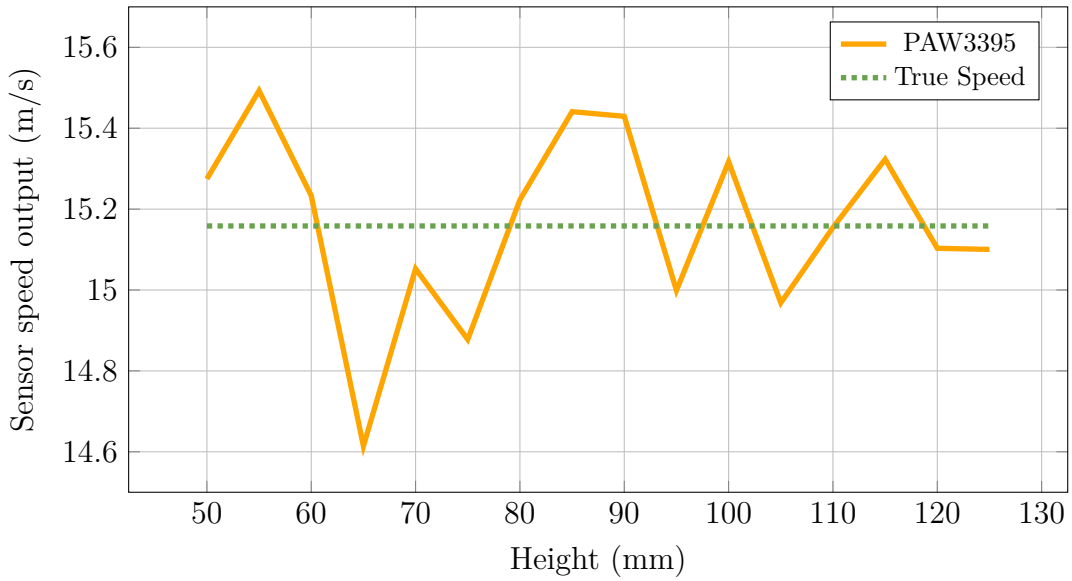

Figure 4.8: Speed ratio fitted polynomial multiplied with measured speed on different heights.

4.2.4 Impact of Pinhole Cover on Sensor Output

The following results presented as box plots in Figure 4.9 were obtained by testing PAW3395 with and without the pinhole cover at two different speeds, 100 RPM and 1000 RPM, corresponding approximately to 3 m/s and 30 m/s respectively.

Tests were done with both 20 W and 40 W of IR illumination using the test rig with the wheel mounted to a motor. See Figure 3.10. The deviation across 1000 measurements for the different configurations can be seen in Figure 4.9 and 4.10.

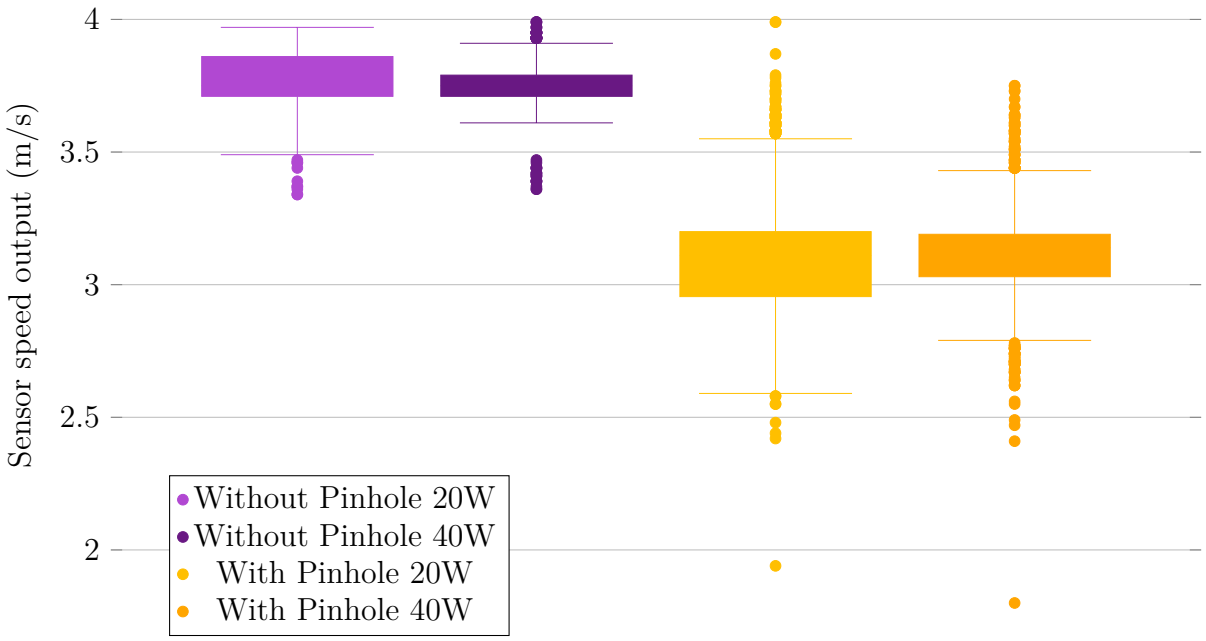

Figure 4.9: Sensor deviation for PAW3395 with and without pinhole at 20 W & 40 W for 100 RPM.

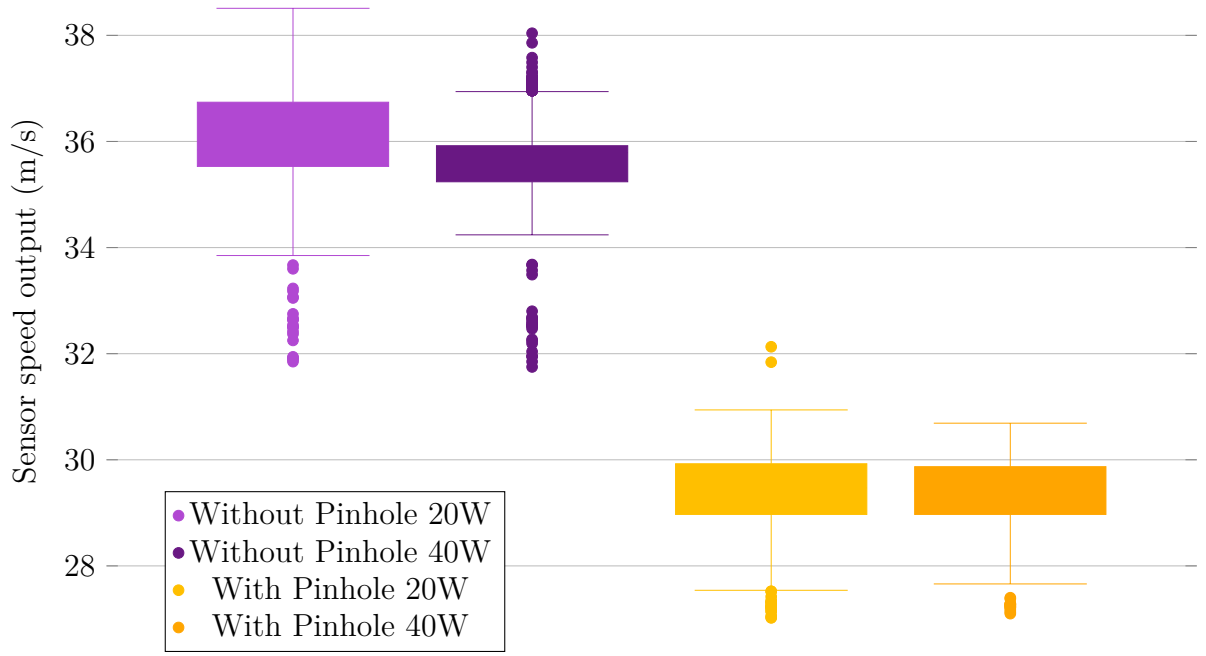

Figure 4.10: Sensor deviation for PAW3395 with and without pinhole at 20 W & 40 W for 1000 RPM.

4.2.5 Testing on Asphalt

In Figure 4.11, the speed measurements of a quick acceleration and deceleration are presented. This corresponds with the movement of the trolley and shows that the sensor is capable of reading displacement information on asphalt.

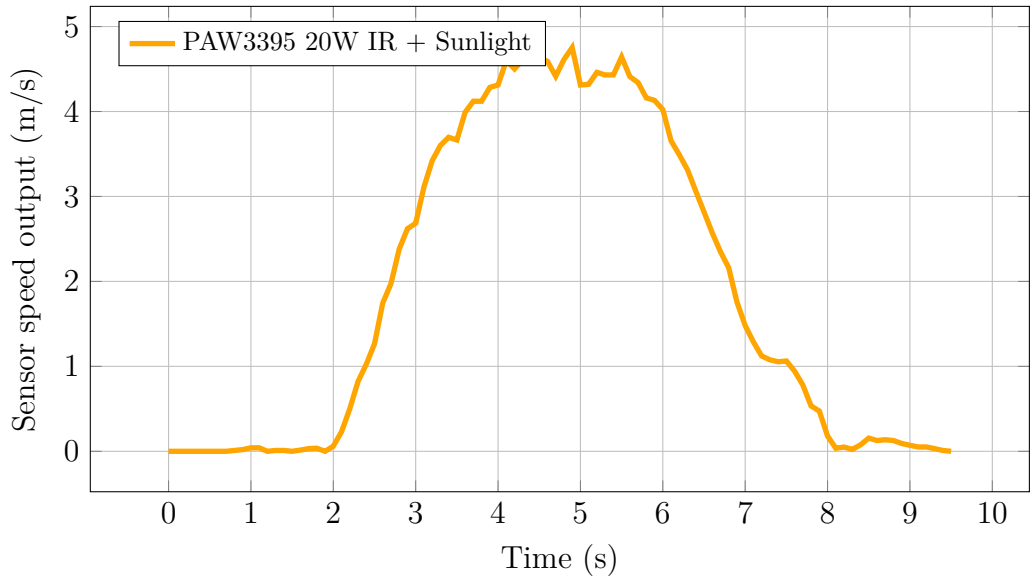

Figure 4.11: Sensor output as a function of time during a short sprint on asphalt.

Figure 4.12 represents the sensor output as a function of time during the driving sequence with the car. Due to ground clearance limitations, no external lighting solution was used, sunlight therefore served as the sole light source. Initial acceleration up to a cruise control speed of 120 km/h ($\approx$ 117 km/h using GPS) as well as deceleration can be seen.

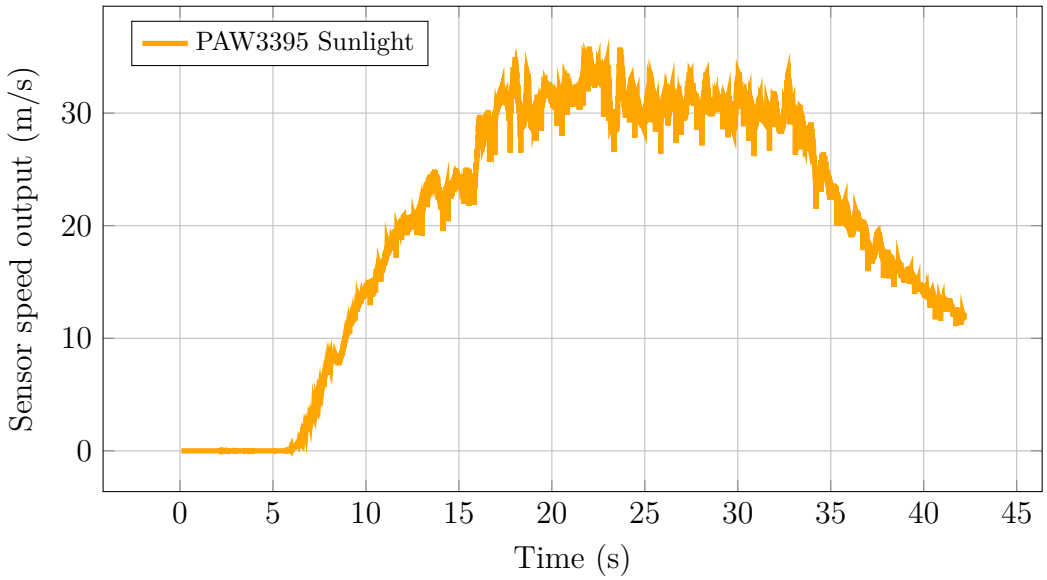

Figure 4.12: Sensor output as a function of time during a driving sequence with the car and sunlight as illumination.

In Figure 4.13 below, the deviation across 1000 measurements taken during the part of the driving sequence where a constant speed was held is compared with those obtained under a controlled environment using the electric motor test rig, seen in Figure 3.10.

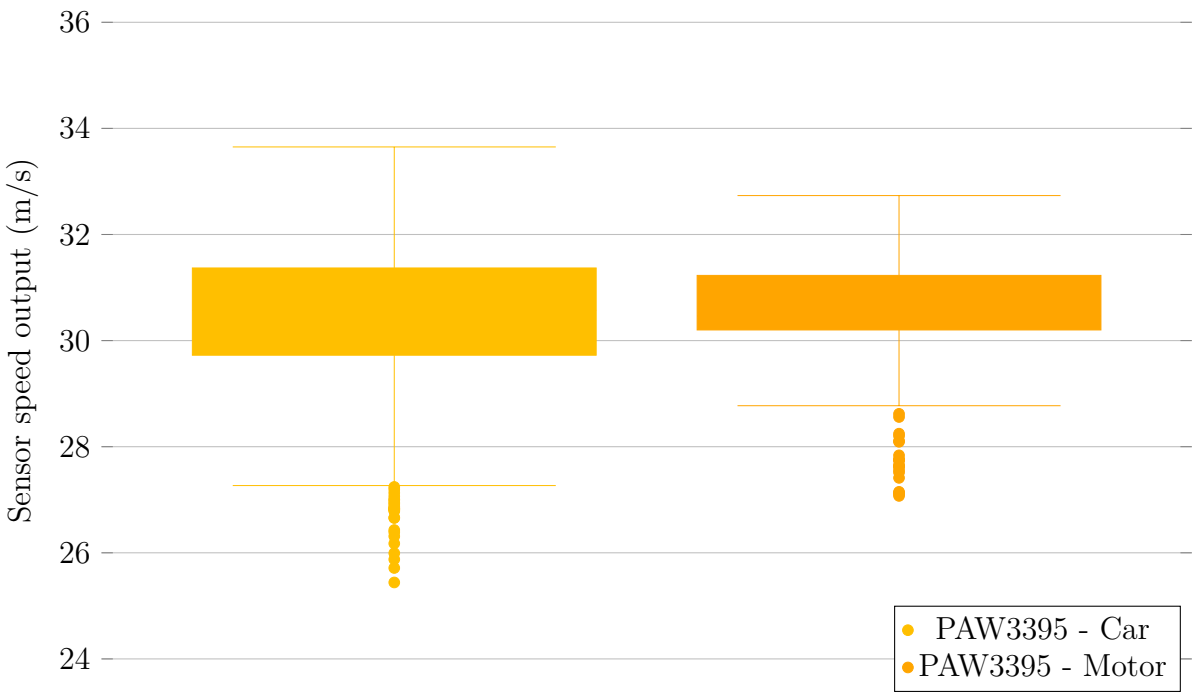

Figure 4.13: Sensor deviation comparison, data from testing on the car and the wheel with the PAW3395.

4.3 Final Design

The final design for the NGSS prototype, with a weight of 267 g, is shown as an exploded view in Figure 4.14. The housing consists of a 3D printed PLA top and bottom enclosure, assembled using M4 bolts and nuts. The top enclosure has a cut-out in the side to enable the power and CAN connectors for the PCB. The bottom enclosure has a cut-out where a glass protective cover was placed, allowing the lens to look through it. The optical lens is screwed into the 3D-printed PLA middle part. The PCB is secured on the same plate with M2 screws.

A light source is not integrated into the NGSS. For the final testing, the lighting solution consisted of a 40 W IR LED, mounted on a heat sink and placed beside the NGSS. The light was directed toward the ground. In some tests, the sunlight was used as the only lighting source.

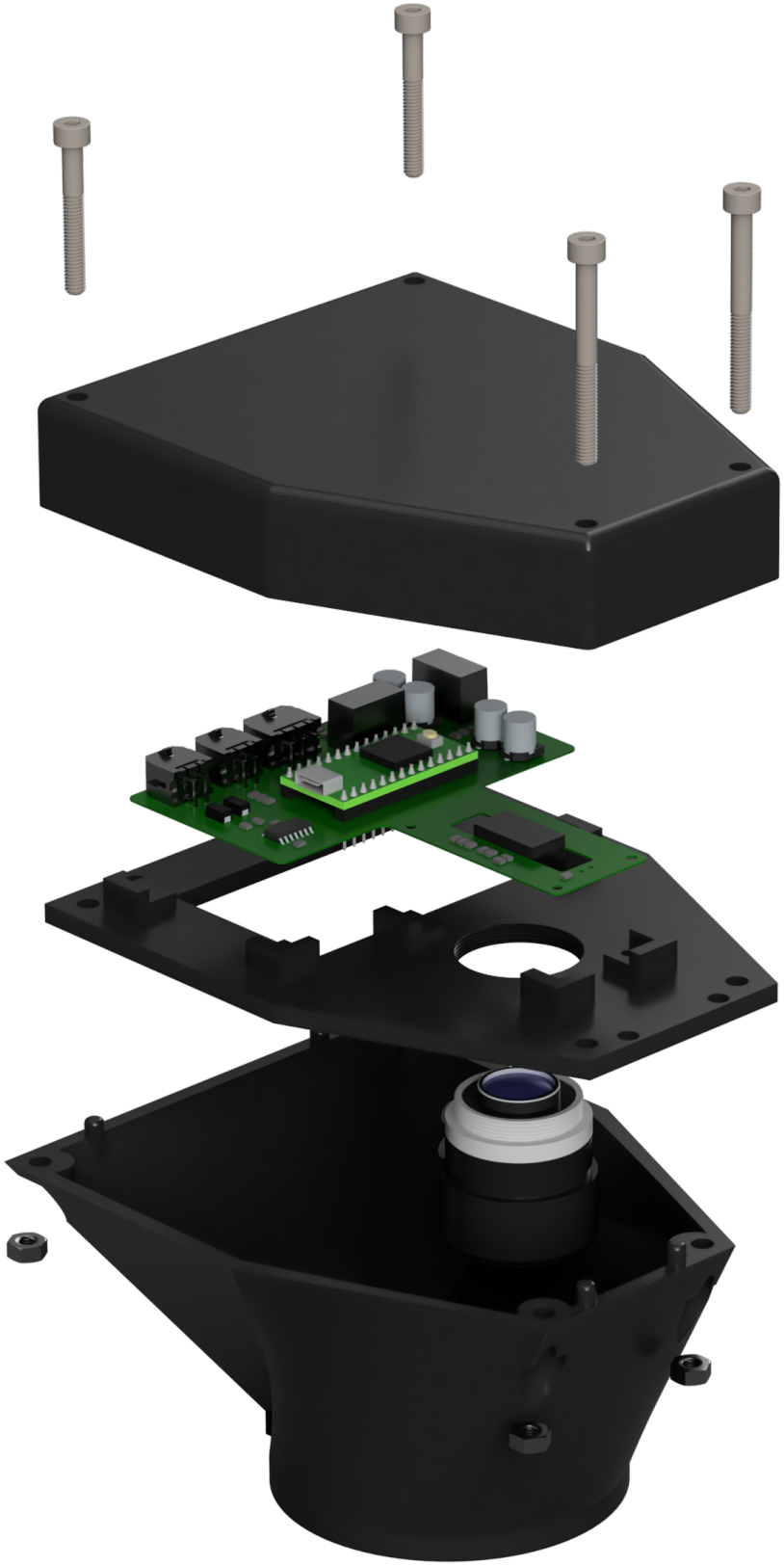

Figure 4.14: Rendered exploded view of the finished NGSS prototype.

5

Discussion

This chapter discusses the findings from testing, the methodology used, experimental uncertainties, ethical aspects of this project, and potential future work. It examines the performance of the NGSS and considers possible improvements to the method.

5.1 Test Outcome

This section will discuss and compare the results from the individual tests that were presented in previous sections, as well as potential causes and contributing factors.

5.1.1 Assessing Sensor Linearity Across Speed Range

From the sensor speed output in Figure 4.1, it can be seen that the sensor PAW3395 has a linear relationship between the surface speed and output. PMW3360 has similar behaviour but has some deviations as the surface speed increases. This also means that PAW3395 is the more reliable option out of the two sensors and would be the more suitable choice in terms of accuracy for the NGSS.

Both sensors were calibrated against the actual surface speed. As seen in Figure 4.2, the calibration, as expected, improved the accuracy of the output. However, the output speed remains imperfect during the validation run. This is likely due to minor fluctuations in the wheel speeds and tachometer inaccuracies, which would affect both the calibration and validation processes. The highest observed deviation of $\approx 1\,\mathrm{m/s}$ would correspond to an error margin of $\approx 3\,\%$ at $120\,\mathrm{km/h}$.

5.1.2 Evaluation of Light Sources

From the results seen in Figure 4.4 and in Figure 4.5, a clear difference in sensor performance can be seen between the two displacement sensors with different lighting solutions. When the light intensity increases, the variance in the output decreases for both displacement sensors. A clear improvement in performance can be seen for the PMW3360 at 1000 RPM, when the 500 W floodlight is being used. However, this is not as noticeable as looking at the PAW3395, which only slightly benefited from more light. Even if a clear improvement is seen in the PMW3360 at 1000 RPM, the accuracy is still inadequate when compared to the PAW3395, which has more accurate readings for all different light sources. Notably, no lens was used on the 40 W or 20 W IR LEDs, which resulted in

some light scattering. Using a lens to concentrate the light, similar to a spotlight, could potentially improve the results and reduce the difference in performance between the two IR lighting solutions.

An interesting observation is also the inconsistencies between more light and better performance for the lower surface speed of 100 RPM. A presumable cause for this is the built-in auto-exposure feature of both displacement sensors. The displacement sensors, therefore, have full control over the shutter time and, thus, the overall exposure of the image. With this being an unknown, it could theoretically fail to expose properly, resulting in worse-quality images, which could lead to more unreliable displacement calculations. For higher surface speeds and more light, the displacement sensor might be forced to use a faster shutter time, which, with enough light, would result in images with less noise and more easily differentiable surface features. This might be the reason why the PAW3360 has acceptable deviation with enough light at 1000 RPM. With this in mind, it can be concluded that the variance in the output speed of the NGSS decreases when the ground is illuminated with more light.

To summarise, the PAW3395, as expected, performed better in all of the cases. A better illuminated surface resulted in better performance when it comes to light. For the PAW3395, 20 W IR LED worked, but the accuracy could, as suggested, always be improved with more light. This might, however, not always be possible depending on implementation. Other alternatives, such as concentrating the light, could be a viable solution.

5.1.3 Height and Focus Evaluation

As seen in Figure 4.6, the image focus has to be within a certain threshold to be able to calculate displacement. Reasons for not being able to read at distances less than 40 mm could be that the optics are not made to accommodate such short distances, resulting in unusable image data. Given more time, this could be investigated further to determine whether that is the case or not. However, it was also shown that the height affected the sensor output when used at the appropriate distances. As expected, a greater height yields less relative displacement per unit of distance in the direction of movement. This is illustrated in Figure 4.6, where in the interval of 50 mm to 125 mm the speed output decreases as height increases. Therefore, as Figure 4.7 shows, a trend line can be fitted and used to correct the speed output within this interval.

5.1.4 Impact of Pinhole Cover on Sensor Output

In both Figure 4.9 and Figure 4.10, there is an offset between the measurements taken with and without a pinhole. This is caused by optical changes which affect the calibration of the sensor and can therefore be ignored. It is, however, clear from Figure 4.9 that the pinhole cover negatively affects the reliability of the sensor since the variance is much larger. In Figure 4.10, the same test was conducted but at a wheel speed of 1000 RPM. At higher speeds, the difference between the sensor with and without the pinhole is much less, the general tendency is however still there, suggesting the removal of the pinhole cover.

5.1.5 Testing on Asphalt

As seen in Figure 4.11, the sensor output clearly follows the shape of what would be expected for this type of test. Although the sensor was not calibrated, this suggest that the sensor works as intended without any unexpected measurement errors. Figure 4.12 also has the expected shape. Although some noise can be seen, it still shows that the sensor is capable of measuring speed up to $\approx 33\,\mathrm{m/s}$ in conditions similar to those of the race car.

The comparison shown in Figure 4.13, as expected, shows that the real-world driving data has a slightly higher deviation. This is likely due to factors such as slight fluctuations in vehicle speed, but also road irregularities. Although some deviation was observed, the overall difference in deviation is not that large. Since the test rig should have a limited amount of deviation due to consistent speed and surface, the results indicate that most deviation comes from the sensor rather than external factors.

5.1.6 Selecting Hardware

Based on the tests conducted, some key design choices were made. The linearity of both sensor outputs provided a clear indication of which displacement sensor would yield the most consistent results. The main concern throughout the project was whether a sufficient lighting solution could be implemented for the PAW3395 to function correctly. If not, the PMW3360 could have been used, due to it being less demanding of light. This would, however, be a less favourable option, as it performed worse in almost all of the tests conducted. The tests evaluating lighting, however, showed that it is definitely possible to use the PAW3395. The test evaluating the impact of the pinhole indicated that it should be removed. For the final design of the prototype, the PAW3395, without a pinhole cover, was selected.

When it comes to the light, due to the sheer amount needed, it was decided not to integrate it with the sensor design. The test showed that more light benefited the accuracy. A 500 W halogen floodlight would not be a viable option. Tests with both 20 W and 40 W IR LEDs showed great results, it is therefore recommended to choose a solution within this range, depending on the use case, ground clearance needed, mounting needs and possibilities of concentrating the light onto the surface.

5.2 Fulfilment of CFS Requirement

At the start of this project, requirements for the NGSS were provided by CFS, shown in Section 1.2. When it comes to performance, the NGSS is capable of measuring speeds from 0 km/h to at least $\approx 120\,\mathrm{km/h}$ and it is done with an output refresh rate of 100 Hz. The sensor outputs speed measurements in both X and Y over CAN as requested, but yaw-rate was not implemented as defined by the project's delimitations. An error margin of 1 % to 2 % was also requested, an estimated error is at least 3.5 %, the main focus was however not to minimise this and could with further calibration and adjustments be improved.

Other requirements that were wished, such as being able to tolerate squat and movement of the car, not requiring calibration between ride height changes, tolerating electrical interference and vibrations, as well as passing the water spray test at competitions, should all be doable with modifications if needed, but have not been tested. This may include adding a height sensor, swapping the lens for one with auto focus and sealing the enclosure using gaskets among other. Another request that has not been tested is how the sensor reacts to reflective surfaces such as water puddles. A known issue with some computer mice are normal reflective or opaque surfaces, so this might be a problem that has to be investigated further.

5.3 Choice of Method

To determine the most suitable method for measuring ground speed, a literature study was first conducted. A Pugh matrix was used to formally evaluate and compare different potential solutions. The Pugh matrix enabled a structured comparison, but it is not entirely free from bias. All the criteria, the criterion weights and the scoring are all done manually by the group. As a result, the outcomes may have unintentionally been influenced by bias. A more objective approach would have been to involve different people when creating the matrix and scoring the solutions. Nevertheless, some level of bias in the final scoring is inevitable, no matter how carefully it is being done.

After a decision was made on what method to use, hardware had to be selected. Since displacement sensors are not meant to be used in this way, the general method used during development was to continuously compare and test. To begin with, it was important to try displacement sensors with different specifications to understand their limitations and capabilities for this type of implementation. Another reason for trying multiple displacement sensors is that they require different amounts of light. In this way, multiple lighting solutions could be evaluated based on both sensors, with different baselines. Although more displacement sensors could have been tested, the two selected ones were enough to get an understanding of how the specifications affected the possibilities of implementing them for this use case.

When comparing measurement data, most comparisons focused on the amount of deviation the sensor would output for constant speeds during a set time frame. Using a constant speed and taking 1000 measurements should give each of the configurations a fair comparison. Although these can be plotted over time, the difference might be hard to notice in some cases. Box plots were therefore a better alternative, as they show the distributions of the values outputted by the sensor for all the measurements, and the sensor behaviour can be more easily compared. The limitations with box plots are, however, that it is hard to detect temporal fluctuations, noise patterns or similar.

5.4 Comparison to Other Projects

Other works have also used displacement sensors to measure velocity. In [44], He *et al.* tested the ADNS-2610 sensor, which has a lower resolution (400 CPI) and slower tracking speed (12 IPS) compared to PAW3395 (26,000 CPI and 650 IPS). While their study did not focus on maximising sensor speed, they proved that optical flow can measure ground speed, showing that this method works.

Other works use alternative methods to measure ground speed that are aimed at being used for FS cars. Albrecht *et al.* used a radar-based technology to measure ground speed [4], which is described in Section 2.2. They achieved a speed accuracy of $\pm$ 0.5 km/h which is lower then the one from this project, $\pm$1.04 m/s corresponding to $\pm$3.74 km/h. Their speed accuracy is based on testing on asphalt, while the accuracy tests in this project were conducted under controlled circumstances (see Figure 3.10). However, their work involved higher complexity, such as custom 3D printed lens assemblies, which is beyond the knowledge of the group. In addition, components that are difficult to acquire were used, for instance, the radar module used is no longer available.

5.5 Sources of Error

Several uncertainties may have affected the accuracy of the speed measurements and calibration of the NGSS. The displacement sensors benefit from a strong and consistent light source. Inconsistent, misplaced or ambient external light can affect the sensor's measurements, causing deviations in the speed output. Additionally, there is no indicator for when the displacement sensor is optimally focused through the lens, which can lead to variation in the reading capability. As a result, when remounting the two displacement sensors between the tests, differences in focus, height, and light can occur from test to test, which can contribute to variations in the results.

The vertical displacement caused by tire deformation, a rough and irregular surface, or suspension movement leads to an alternation in the displacement sensor's distance to the ground. Since the PAW3395 and PMW3360 sensors were only calibrated on the fixed mounting height 80 mm, such variations can result in an incorrect calibration factor making the output speed inaccurate.

The surface texture also has an important role in the speed measurement accuracy. The NGSS has only been calibrated on sandpaper, which was chosen as the closest material resemble the asphalt's surface, although the sandpaper reflects more light than asphalt. The sensor has been tested on actual asphalt and gives a speed output, but the accuracy has not been tested. Different asphalt types have varying grain size and reflectivity, which can affect the displacement sensor's ability to read the surface. In addition, water, dust or debris beneath the CFS car may cause the displacement sensor to measure the speed of those rather than the actual surface the vehicle is driven on, leading to inaccurate speed data.

5.6 Further Work and Research

While this project is finished, many challenges still remain for this prototype to fully function as an NGSS alternative. Further development and testing with accurate validation tools, to both calibrate and further detail investigate how changes in height, image focus, image brightness and speed affects the displacement output would still be needed. The possibility of running the sensor at a higher frequency than 100 Hz also exists, which would allow for data sampling and should be explored further. How well the sensor performs under real-world conditions, such as wet conditions and when subject to vibrations, uneven surfaces or surfaces with debris, should also be tested. Parts of the design have a lot of areas that could be changed. As of now, the lighting solution is seen as an external part and was not incorporated into the sensor, although this was the idea to begin with. The reason for this was the size, cooling and power consumption needed for the IR LEDs that were used. To prevent this from being an issue, either lenses which concentrate light on the specific area of interest or different lighting solutions could be tested. This could ease the process of integrating a sufficient light source into the sensor unit, making it a complete solution.

Considering the further development needed for a fully functional NGSS, we suggest that this project should be a bachelor's thesis at Chalmers next year. The current method using displacement sensors could be further evaluated to determine whether it can eventually become a viable alternative. Additionally, alternative approaches, as those discussed in the early stages of this project, could also be explored in future work. Among these, the radar-based solution was the second most promising in our method evaluation and showed significant potential. While a radar-based approach may be more complex, it could be well suited for a master's thesis, offering students with more experience and technical expertise the opportunity to develop an NGSS, and may include real-world testing, mounting the sensor on a car to be tested on track.

5.7 Ethical Aspects

Since the NGSS does not directly interact with people or the environment, it has minimal ethical implications on its own. However, ethical concerns arise when the sensor is used together with other devices. The following paragraphs will therefore focus on the ethical implications on society of the devices that utilise the NGSS.

One area the sensor can be a part of is autonomous vehicles, and there are multiple ethical aspects surrounding this area. With a ground speed sensor, autonomous vehicles can have a more precise representation of their surroundings, which improves overall driving. Another example is improving anti-lock braking systems for better slip calculations, increasing safety. In this way, the sensor could have a positive effect on society. If multiple autonomous vehicles had ground speed sensors, they would all have more precise information about their speed, especially in unusual situations such as emergency braking when the car slides. By integrating this technology in conjunction with communications technology that allows the cars to share their speeds, such as in a smart integrated grid, they would not always have to rely on their own sensors to estimate the speed of the

vehicles around them. This would allow a car to adjust its speed based on surrounding vehicles, introducing another way of preventing collisions and navigating traffic with higher precision.

Another dilemma to consider would be the use of the low-cost NGSS for military applications. Autonomous drones are used at an increasingly higher rate in today's warfare, and a low-cost NGSS would make these drones cheaper and more accurate. Considering the fact that these NGSS can also be made very lightweight and take up minimal space, such systems could be deployed more extensively.

Even if the NGSS itself may not have a lot of ethical aspects directly tied to it, the things it will be a part of do. In the examples previously discussed, some risks were mentioned. However, it will also be used in a good way, for example, to help improve safety systems, thus positively impacting society.

6

Conclusion

The purpose of the project was to evaluate different solutions for an NGSS and to develop a prototype that eventually could be implemented in a future CFS vehicle. Various ground speed measurement methods were studied and evaluated based on multiple criteria set by the project group. Accessibility, complexity, and the requirements from CFS were considered to be the most important aspects to evaluate. From this, an optical solution based on displacement sensors was selected as the method for further development, as it was evaluated to be the most suitable for this project. Two displacement sensors, PAW3395 and PMW3360, were purchased, a PCB was designed, and software was developed. In the end, a working prototype NGSS was constructed.

Testing showed that the PAW3395 sensor is the more reliable option out of the two. Speed measurements at 100 Hz under controlled environments were successfully conducted at speeds to up 120 km/h, with a estimated error margin below 3.5 % after calibration. The NGSS was also tested under real-world conditions mounted on a car, showing great results for speed measurements from 0 to 120 km/h, as requested by CFS. These results prove that the chosen method could be a viable low cost option if developed further. When it comes to future work, testing with accurate validation tools are necessary to improve and evaluate how well this method works for these types of speed measurements. Other changes included, integrating a lighting solution into the module for a complete solution. It is therefore recommended to have this project as a Bachelor's thesis next year, or even possibly a Master's thesis

Bibliography

[1] Taylor, D., Thoman, G., and Maschino, D., "Practical Electric Speedometer System for Passenger Car Applications," *SAE Technical Paper 830326*, Feb. 1983, doi:10.4271/830326.

[2] L. Cocco, s. Rapuano, "Accurate speed measurement methodologies for formula one cars," in *2007 IEEE Instrumentation Measurement Technology Conference IMTC 2007*, Warsaw, Poland, 2007, pp. 1, doi: 10.1109/IMTC.2007.379160.

[3] C. Xu, L. Daniel, E. Hoare, V. Sizov and M. Cherniakov, "Comparison of speed over ground estimation using acoustic and radar Doppler sensors," in *2014 11th European Radar Conference*, Rome, Italy, 2014, pp. 189-192, doi: 10.1109/EuRAD.2014.6991239.

[4] N. C. Albrecht, D. Langerand, and A. Koelpin, "A fully integrated radar-based true-speed-over-ground sensor for highly dynamic road vehicles," in *2024 IEEE/MTT-S International Microwave Symposium - IMS 2024*, 2024, pp. 398-401, doi:10.1109/IMS40175.2024.10600256.

[5] S. Wrobel, M. Ahmadian, M. Craft and J. Munoz, "Multifunction LIDAR Sensors for Non-Contact Speed Measurement in Rail Vehicles: Part 2 — Data Collection and Analysis," in *2013 Joint Rail Conference*, 2013, doi: 10.1115/JRC2013-2500.

[6] W. Fu, S. Hu, C. Luo, Y. Li, S. Guo and J. Zhang, "Development and Test of GNSS/IMU-Based Speed Measurement Device for Agricultural Machinery," in *11th International Conference on Computer and Computing Technologies in Agriculture (CCTA)*, Jilin, China, Aug. 2017, pp. 440-451, doi: 10.1007/978-3-030-06137-1_40.

[7] D. Lhomme-Desages, C. Grand, F. B. Amar and J. C. Guinot, "Doppler-Based Ground Speed Sensor Fusion and Slip Control for a Wheeled Rover," in *IEEE/ASME Transactions on Mechatronics*, vol. 14, no. 4, pp. 484-492, Aug. 2009, doi: 10.1109/TMECH.2009.2013713.

[8] D. Bohl, N. Kariotoglou, A.B. Hempel, P.J. Goulart and J. Lygeros, "Model-based current limiting for traction control of an electric four-wheel drive race car," in *2014 European Control Conference (ECC)*, Strasbourg, France, 2014, pp. 1981-1986, doi: 10.1109/ECC.2014.6862532.

[9] S. Premnath, S. Mukund, K. Sivasankaran, R. Sidaarth and S. Adarsh, "Design of

an autonomous mobile robot based on the sensor data fusion of lidar 360, ultrasonic sensor and wheel speed encoder," in *2019 9th International Conference on Advances in Computing and Communication (ICACC)*, Kochi, India, 2019, pp. 62-65, doi: 10.1109/ICACC48162.2019.8986199.

[10] J. Stephant, A. Charara and D. Meizel, "Experimental validation of vehicle sideslip angle observers," in *IEEE Intelligent Vehicles Symposium*, Parma, Italy, 2004, pp. 150-155, doi: 10.1109/IVS.2004.1336372.

[11] Institution of Mechanical Engineers, "Formula student," [Online]. Available: https://www.imeche.org/events/formula-student (accessed on: 2025-02-26).

[12] Chalmers Formula Student, "2024 team," Chalmers Formula Student. [Online]. Available: https://www.chalmersformulastudent.se/2024-team (accessed on: 2025-03-10).

[13] Formula Student Germany, 2024. "Results FSG 2024," Formula Student Germany. [Online]. Available: https://www.formulastudent.de/fsg/results/2024 (accessed on: 2025-03-18).

[14] S. Yoo, and Chalmers Formula Student, 2024. [Picture]. Unpublished.

[15] Formula Student Germany, "Formula student rules 2025," Formula Student Germany. [Online]. Available: https://www.formulastudent.de/fsg/rules (accessed on: 2025-03-03).

[16] E. S. Ege, F. Cetin and C. Basdogan, "Vibrotactile feedback in steering wheel reduces navigation errors during gps-guided car driving," in *2011 IEEE World Haptics Conference*, Istanbul, Turkey, 2011, pp. 345-348, doi: 10.1109/WHC.2011.5945510.

[17] A. Dumitrascu and T. Rodica, "Integrated ins-gps system for performance analysis in motorsports," in *2022 29th Saint Petersburg International Conference on Integrated Navigation Systems (ICINS)*, 2022, pp. 1-2, doi:10.23919/ICINS51784.2022.9815345.

[18] T. O'Kane and J. V. Ringwood, "Vehicle speed estimation using GPS/RISS (Reduced Inertial Sensor System)," in *24th IET Irish Signals and Systems Conference (ISSC 2013)*, Letterkenny, 2013, pp. 1-6, doi: 10.1049/ic.2013.0046.

[19] Kistler, "Non-contact optical sensors correvit SFx-F1/2067A," Kistler. [Online]. Available: https://www.kistler.com/SE/en/cp/non-contact-optical-sensors-correvit-sfx-f1-2067a/P0001261 (accessed on: 2025-02-28).

[20] Sensoric Solutions, "Optical sensor systems," Sensoric Solutions. [Online]. Available: https://www.sensoric-solutions.com/products/sensors/ (accessed on: 2025-02-28).

[21] *RADAR II AND III Ground Speed Sensors*, Auburn, IL, USA: DICKEY john, [Online]. Available: https://dickey-john.com/getmedia/62d81cce-8ec6-43d8-8bec-b4ec3a418624/Radar-II-and-III_US_5002001_RevC_Web_1.pdf (accessed on: 2025-02-28).

[22] M. A. Richards, J. A. Scheer and W. A. Holm, *Principles of Modern Radar Vol. I:*

Basic Principles, D. R. Kay, Edison, Ed., NJ, USA: SciTech Publishing Inc, 2010, ch. 4, pp. 274-275.

[23] F. B. Berger, "The nature of doppler velocity measurement," *IRE Transactions on Aeronautical and Navigational Electronics*, Pleasantville, NY, USA, 1957, pp. 104, doi: 10.1109/TANE3.1957.4201534.

[24] K. Shariff, E. Hoare, L. Daniel, M. Antoniou, and M. Cherniakov, "Comparison of adaptive spectral estimation for vehicle speed measurement with radar sensors," *Sensors*, 2017, pp. 1, doi: 10.3390/s17040751.

[25] J. Dybedal, "Doppler Radar Speed Measurement Based On A 24 GHz Radar Sensor," Master thesis, 2013, [Online]. doi: 10.13140/RG.2.2.31980.77443.

[26] C. Waldschmidt, J. Hasch, and W. Menzel, "Automotive radar — from first efforts to future systems," *IEEE Journal of Microwaves*, 2021, pp. 135-136, doi: 10.1109/JMW.2020.3033616.

[27] Silicon Radar, *TRA_120_002, 120-GHz Highly Integrated IQ Transceiver with Antennas on Chip in Silicon Germanium Technology*, Frankfurt, Germany, 2018, [Online]. Available: https://siliconradar.com/datasheets/Datasheet_TRA_120_002_V0.8.pdf (accessed on: 2025-04-10).

[28] M. A. Sutton and J. Orteu and H. W. Schreier, *Image Correlation for Shape, Motion and Deformation Measurments*, New York, USA: Springer 2009, ch. 81, 87, pp. 461-466.

[29] R. Szeliski, *Computer Vision, Algorithms and Applications Second Edition*, D. Gries, O. Hazzan, Eds., Cham, Switzerland: Springer, 2022, pp. 337.

[30] R. Labudzki, S. Legutko, and P. Raos, "The essence and applications of machine vision," in *Tehnicki Vjesnik*, 2014, pp. 905-906.

[31] Y. Gao, T. Qiao, H. Zhang, Y. Yang, Y. Pang, and H. Wei, "A contactless measuring speed system of belt conveyor based on machine vision and machine learning," *Measurement*, vol. 139, pp. 127, 2019, doi: 10.1016/j.measurement.2019.03.030.

[32] Open Source Vision Foundation, "Feature matching," [Online]. Available: https://docs.opencv.org/4.x/dc/dc3/tutorial_py_matcher.html (accessed on: 2025-02-28).

[33] Open Source Vision Foundation, "Template matching," [Online]. Available: https://docs.opencv.org/4.3.0/de/da9/tutorial_template_matching.html (accessed on: 2025-02-28).

[34] T. Hossler, "Where's Waldo? A Deep Learning approach to Template Matching," [Online]. Available: https://cs231n.stanford.edu/reports/2017/pdfs/817.pdf (accessed on: 2025-02-28).

[35] M. Zhai, X. Xiang, N. Lv, X. Kong, "Optical flow and scene flow estimation: A survey," in *Pattern Recognition*, vol 114, China, 2021, pp. 1-3, doi: 10.1016/j.patcog.2021.107861.

[36] J. Gibson and O. Marques, "Optical flow fundamentals," in *Optical Flow and Trajectory Estimation Methods*, Cham, Switzerland: Springer, 2016, ch. 1, pp. 1-5.

[37] P. Muller and A. Savakis, "Flowdometry: An optical flow and deep learning based approach to visual odometry," in *2017 IEEE Winter Conference on Applications of Computer Vision (WACV)*, Santa Rosa, CA, USA, 2017, pp. 624, doi: 10.1109/WACV.2017.75.

[38] Open Source Vision Foundation, "Optical flow," [Online]. Available:https://docs.opencv.org/3.4/d4/dee/tutorial_optical_flow.html (accessed on: 2025-02-29).

[39] G. M. Hassan, "Deformation measurement in the presence of discontinuities with digital image correlation: A review," *Optics and Lasers in Engineering*, vol. 137, pp. 1-4, 2021, doi: 10.1016/j.optlaseng.2020.106394.

[40] T. Mei, "Understanding Optical Mice," [Online]. Available: https://d1.amobbs.com/bbs_upload782111/files_11/ourdev_574024.pdf (accessed on: 2025-02-21).

[41] PixArt Imaging, *PMW3901MB-TXQT: Optical Motion Tracking Chip*, Mar. 2020.

[42] T. Ballard and T. Roach and B. Dyre, "Use of Global Optical Flow Rate and Discontinuity Rate Depends on Their Validity as Determinants of Egospeed," in *Proceedings of the Human Factors and Ergonomics Society Annual Meeting*, vol. 42, no. 22, pp. 1540, Oct. 1998, doi: 10.1177/154193129804202220.

[43] "Sensors," *Mouse Guide*, [Online]. Available: https://sensor.fyi/sensors/ (accessed on: 2025-02-28).

[44] M. He, X. Guo, G. Wang, *Enhanced Positioning Systems Using Optical Mouse Sensors*, vol 8918, Cham, Switzerland: Springer, 2014, pp. 463-474, doi: 10.1007/978-3-319-13963-0_47.

[45] Y. Aizu and T. Azakura, *Spatial Filtering Velocimetry: Fundamentals and Applications*, W. T. Rhodes, Ed., Atlanta, GA, USA: Springer, 2005.

[46] I. Sakai and N.J. Chilton and S.J. Pacaud and R.J. Hazelden, "Development of optical speed-over-ground sensors," *Sensors and actuators A:Physical*, pp. 5-7, Oct. 1992, San Sebastian, Spain, doi: 10.1016/0924-4247(93)80036-G.

[47] H. E. Albrecht, *Laser Doppler and Phase Doppler Measurement Techniques*, Heidelberg, Germany: Springer, 2003, pp. 5, 11, 12, 70-75, 275-283, 287.

[48] Polytec, "Polytec," *Basics of Laser Doppler length and speed measurement*, [Online]. Available: https://www.polytec.com/us/velocimetry/technology (accessed on: 2025-

02-28).

[49] *AD7863 Laser Ground Sensor*, Frankfurt, Germany: A&D Company, 2013, [Online]. Available: https://www.aandd.jp/products/dsp/pdf/lgs_ad7863.pdf (accessed on: 2025-03-12).

[50] "Measurement Principles of LDA," *Dantec Dynamics*, [Online]. Available: https://www.dantecdynamics.com/solutions/fluid-mechanics/laser-doppler-anemometry-lda/measurement-principles-of-lda/ (accessed on: 2025-02-28).

[51] "Fiber-coupled aom (acousto-optic modulator)," *AeroDIODE*, [Online]. Available: https://www.aerodiode.com/product/fiber-coupled-aom/ (accessed on: 2025-03-12).

[52] S. Pugh, "Concept Selection: A Method That Works," in *Creating Innovative Products Using Total Design: The Living Legacy of Stuart Pugh*, D. Clausing and R. Andrade, Eds. MA, USA: Addison-Wesley, 1996, pp. 167–176.

[53] PixArt Imaging, "PAW3395DM-T6QU: Optical Gaming Navigation Chip," PAW3395DM-T6QU, Revised, Aug. 2022.

[54] PixArt Imaging, "PMW3360DM-T2QU: Optical Gaming Navigation Chip," PMW3360DM-T2QU, Revised, Sep. 2016.

Appendix

A Schematic and Components for PAW3395DM-T6QU

Table .1: Table of components for the PCB.

Component	Manufacturer part number
Microcontroller	Teensy 4.0
DC-DC converter from 5 V to 3.3 V	TSR_2-2433
DC-DC converter from 5 V to 1.8 V	TSR_2-0518
CAN transceiver	TJA1048T,118
External LED	L-53ID-5V
Sensor Module	PAW3395DM-T6QU
Supply connector	43045-0400
LED Ring Connector	43045-0400

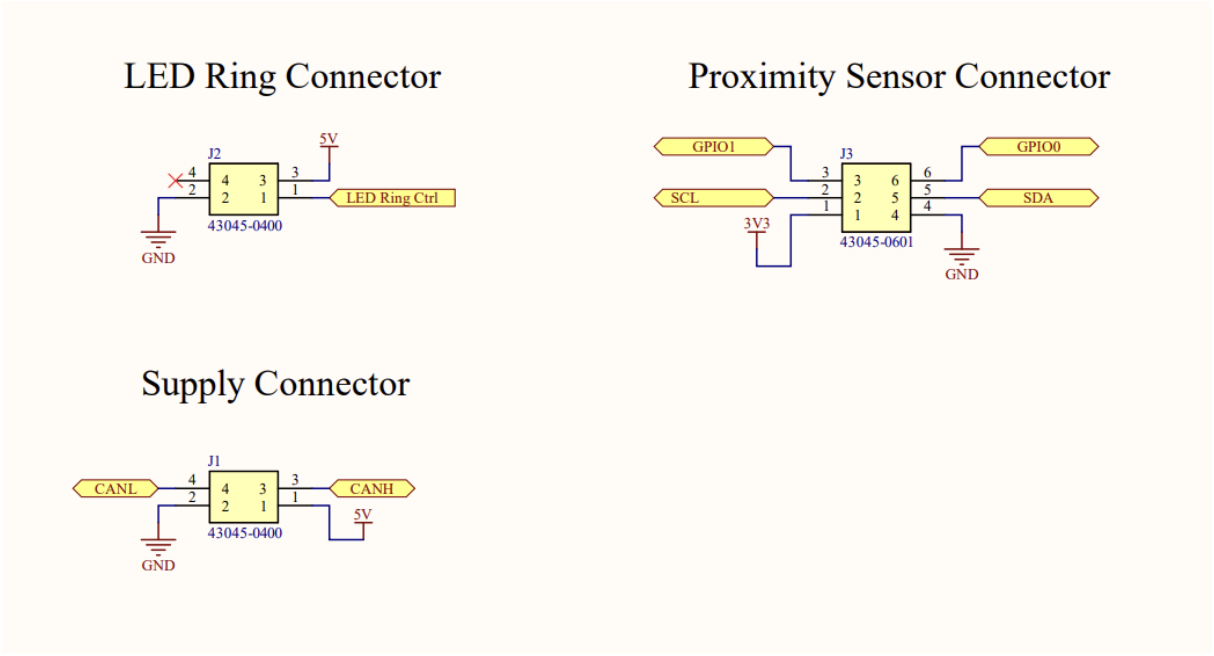

Figure .1: The connector schematics.

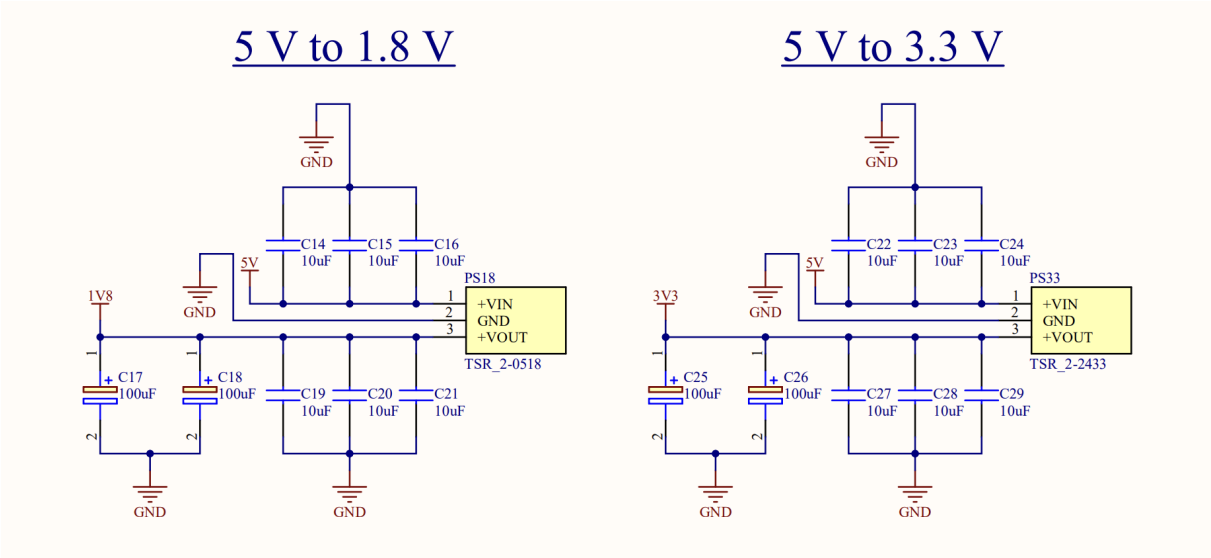

Figure .2: The power distribution schematics.

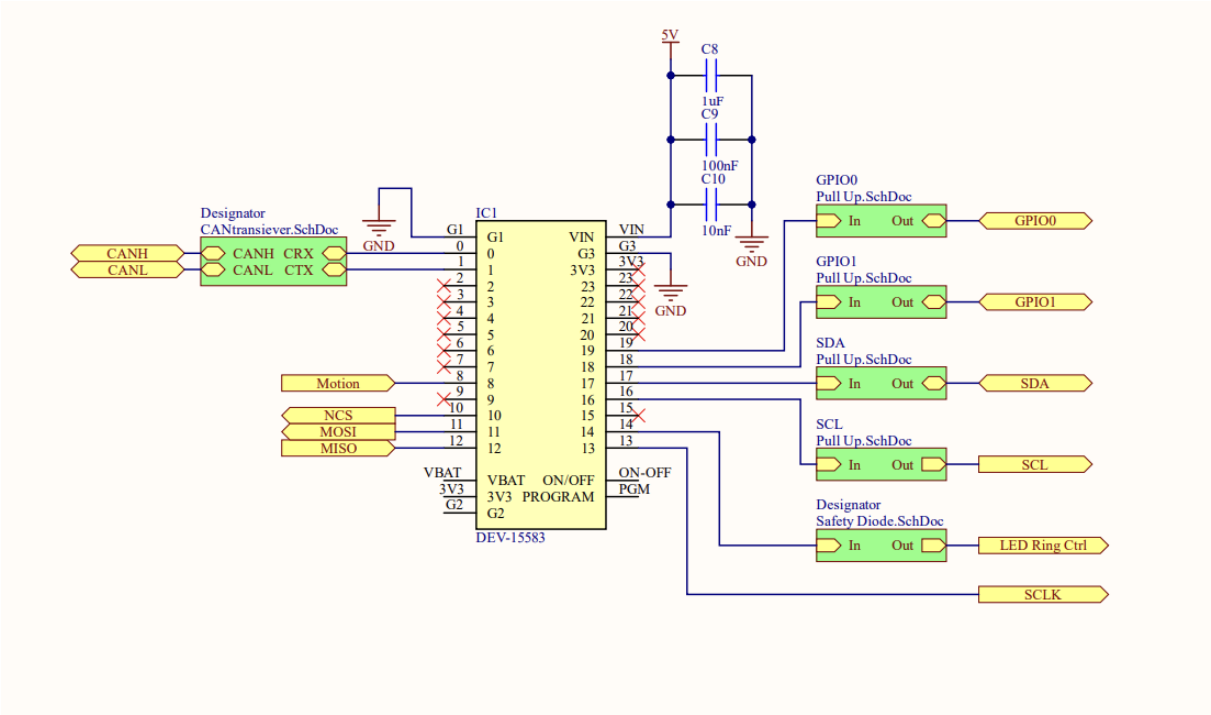

Figure .3: The Teensy schematics.

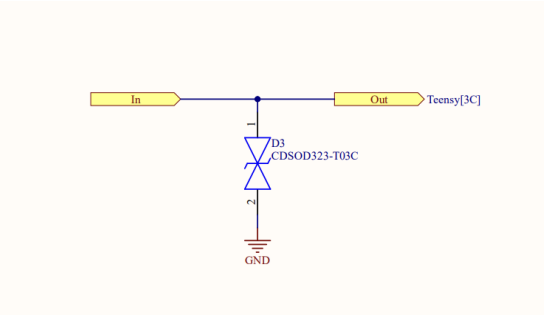

Figure .4: The safety diode sub-schematics.

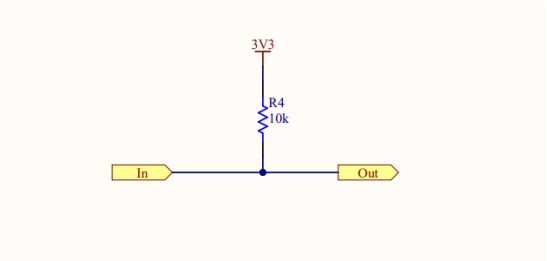

Figure .5: The pull-up sub-schematics.

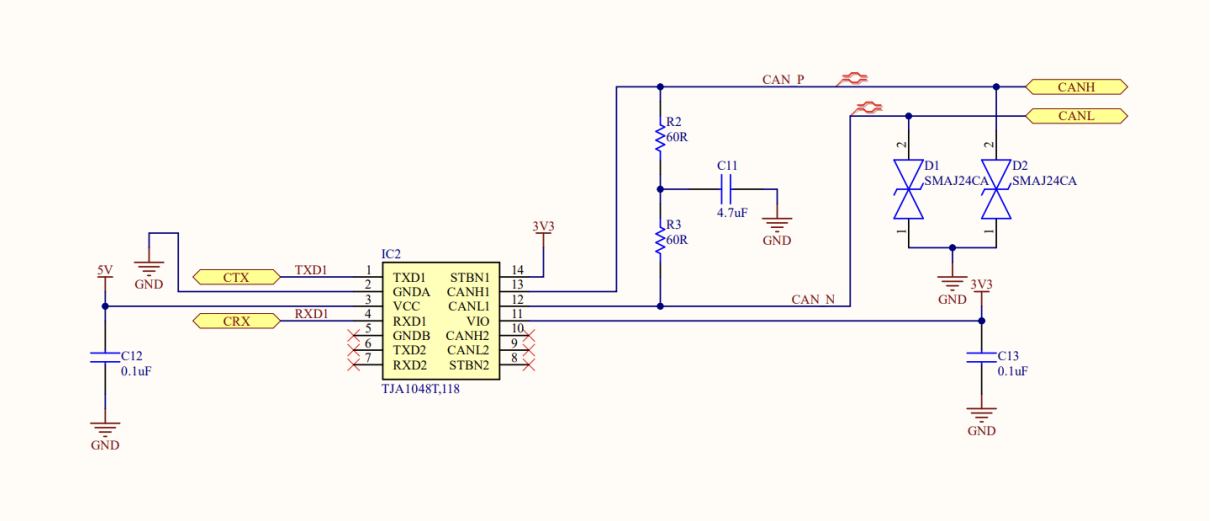

Figure .6: The CAN transceiver sub-schematics.

B Schematic and Components for PMW3360DM-T2QU

Table .2: Table of components for the PCB.

Component	Manufacturer part number
Microcontroller	Teensy 4.0
DC-DC converter from 5 V to 3.3 V	TSR_2-2433
DC-DC converter from 5 V to 1.8 V	TSR_2-0518
CAN transceiver	TJA1048T,118
External LED	L-53ID-5V
Sensor Module	PMW3360DM-T2QU
Supply connector	43045-0400
LED Ring Connector	43045-0400

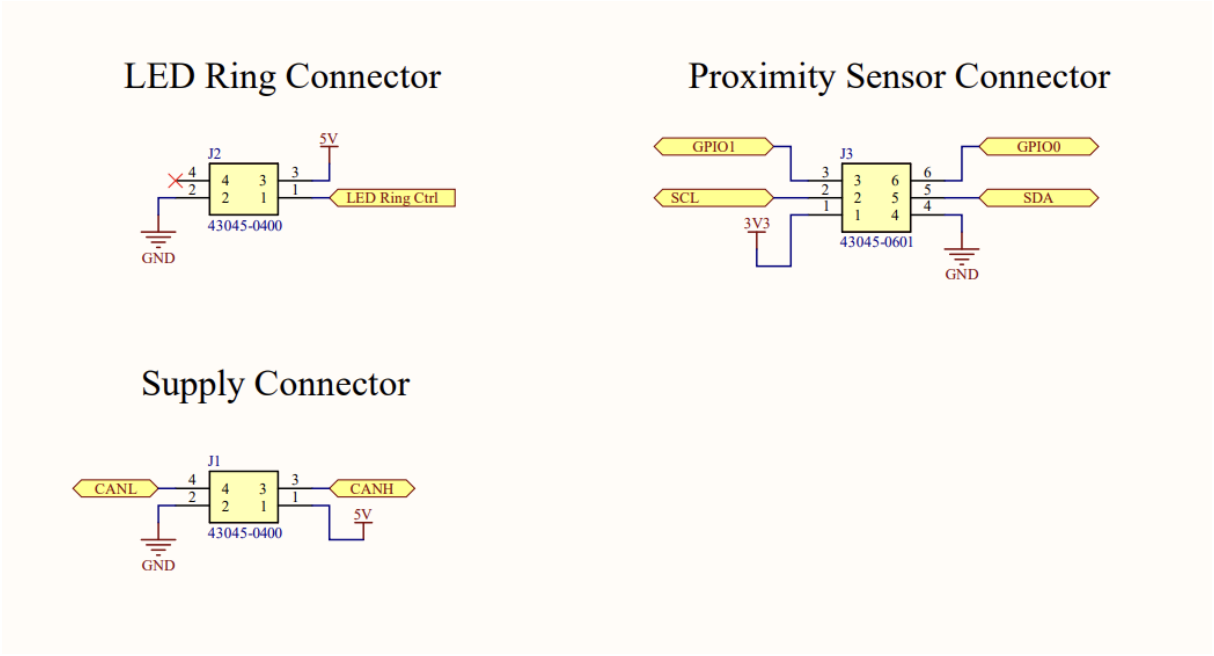

Figure .7: The connector schematics.

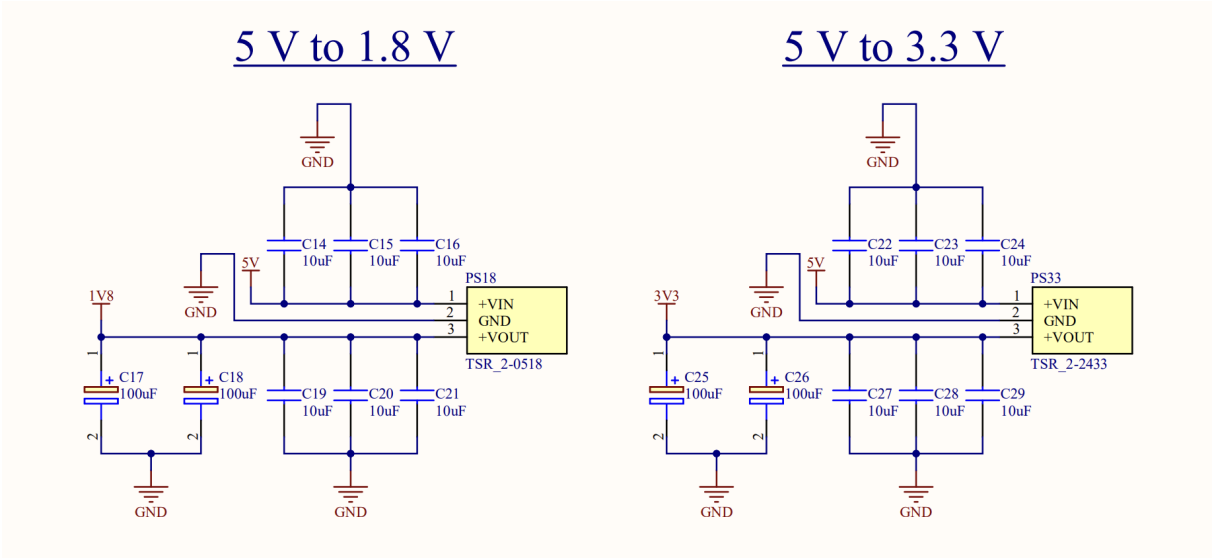

Figure .8: The power distribution schematics.

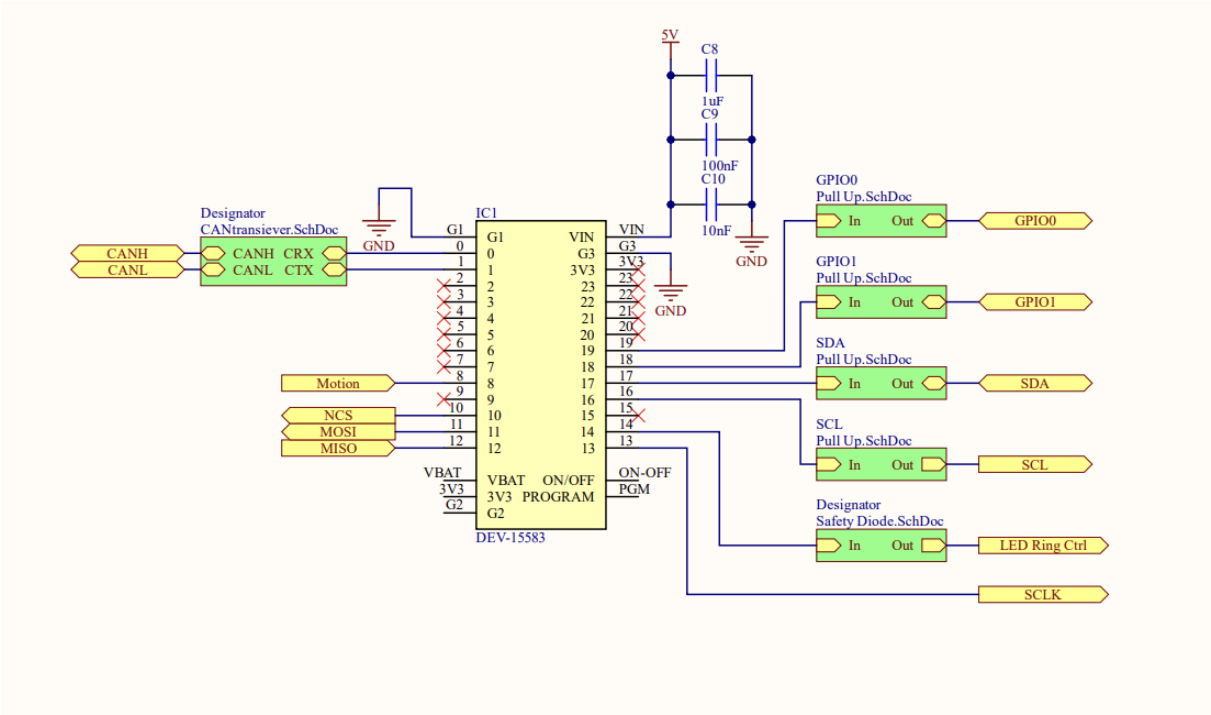

Figure .9: The Teensy schematics.

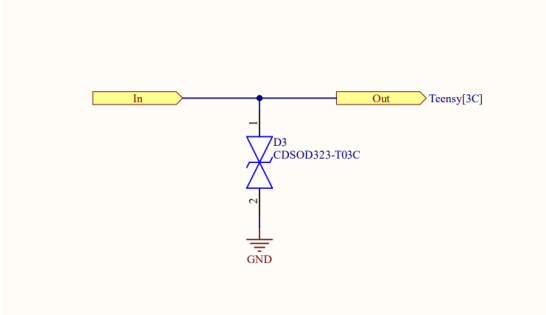

Figure .10: The safety diode sub-schematics.

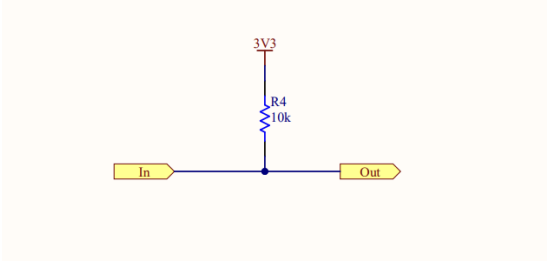

Figure .11: The pull-up sub-schematics.

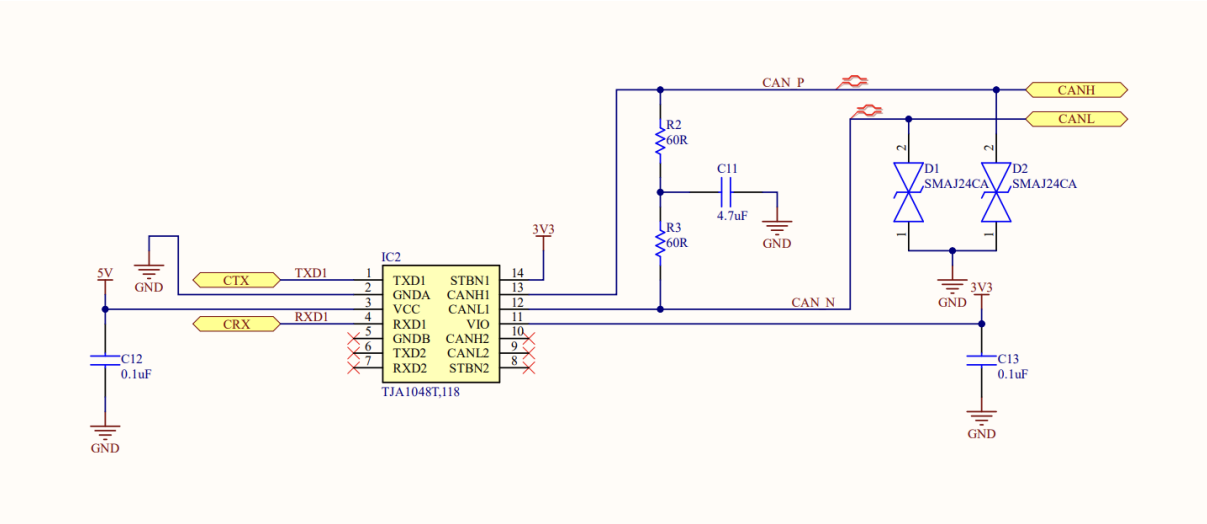

Figure .12: The CAN transceiver sub-schematics.